ULTRAPRECISION DIAMOND MACHINING OF POLYCARBONATE COMPLEX MULTI-SIDED FREEFORM OPTICS

by

Steven M. Swagler

A thesis submitted to the faculty of
The University of North Carolina at Charlotte
in partial fulfillment of the requirements
for the degree of Master of Science in
Mechanical Engineering

Charlotte

2022

Approved by:

_____
Dr. Matthew A. Davies

_____
Dr. Thomas J. Suleski

_____
Dr. Jimmie A. Miller

ABSTRACT

STEVEN M. SWAGLER. Ultraprecision Diamond Machining of Polycarbonate Complex Multi-sided Freeform Optics. (Under the direction of DR. MATTHEW A. DAVIES)

Advances in technology are driving optical systems to become more and more complex and compact. Ultra-precision machining centers have advanced to catch up with optical designs but there is a defined set of methods defining the use of the machines to manufacture complex optics and optical systems. These ultra-precision machines are capable of producing optical surfaces with less than a micrometer of form error and sub-nanometer surface roughness. There are three main methods of ultra-precision manufacturing of optics: diamond turning, ultra precision grinding, and diamond micro-milling. A key advantage of diamond micro-milling is its ability to manufacture surfaces with steep slopes, large sag, and hard to reach areas. The optical systems in head up displays, head worn displays, virtual reality systems, and augmented reality systems push standard diamond turning operations beyond its slope and access capability. These applications are where diamond micro-milling comes in. Optical designs used in the before mentioned applications typically consist of multiple optical surfaces on multiple sides of a single substrate. Machining multiple features on different sides of an optic or optical system remains a challenge. These systems have been manufactured in the past but there is little to no documentation on how these systems were manufactured.

The goal of this is to provide insight on the manufacturing methodology that was developed and used to manufacture complex multi-sided optical systems that require re-fixturing during the manufacturing process. Two optical systems were manufactured. The lessons learned during the manufacturing of the first system were evaluated and changes were implemented for the manufacturing of the second system. Cutting parameters and coolants were tested and developed such that optical sur-

faces could be achieved in a polycarbonate substrate used for prototyping. A surface roughness of 11.7 nm rms was achieved through a developed diamond milling process. The manufacturing methodology developed in this thesis includes diamond milling tool setup, fixturing design, and a manufacturing process which defines how the optical surfaces remain referenced to each other during the re-fixturing of the optical system. A functional multi-sided optical system was successfully manufactured using the defined methodology. Future work includes the development of a metrology methodology for these types of systems and the development of a cost-effective rapid production manufacturing process.

DEDICATION

This thesis is dedicated to all of those who have assisted me in my life journey. Specifically I would like to thank:

My wife, Yadira Swagler for the continued support, love, and patience as I worked to complete my masters degree.

My parents, Brian and Donna Swagler for teaching me all that I needed to become a successful student and member of society. If it wasn't for them, I would not have the great work ethic that I was able to use for the past 6 years as I gained my undergraduate and masters degree.

For all the doctors and nurses that saved my life in the fall of 2021 from three brain bleeds and a TIA. I would not be here today if it wasn't for them.

ACKNOWLEDGEMENTS

I would like to thank:

My advisor Dr. Matthew Davies for introducing me to ultra precision diamond machining, giving me the opportunity to work with him and his research team, and for recommending me for what I consider a dream job.

Dr. Nicholas Sizemore and Dr. Dustin Gurganus for teaching me all that they knew about optics manufacturing and for their patience with all the questions I asked.

Brian Dutterer for teaching and training me on all the manufacturing equipment that I needed to complete this thesis.

Christopher Morgan for answering all my questions and problem solving with me when I ran into problems on the 350 FG.

The Center for Freeform Optics (CeFO) and the National Science Foundation (NSF) for project sponsorship, mentors, and funding.

TABLE OF CONTENTS

LIST OF TABLES

LIST OF FIGURES

CHAPTER 1: INTRODUCTION

The primary objective of this research was to develop a comprehensive procedure for the manufacturing of complex multi sided optical prisms. Through the production of a freeform prism, the procedure was developed, discussed, and tested to ensure manufacturing feasibility.

1.1 Discussion of Ultra Precision Machining History

Ultra Precision machining is the pinnacle of machining. This category of machining is defined by form errors on the order of 100's of nanometers or less and roughness in the 10s of nanometers or less [8]. To satisfy these requirements, both the tooling and machinery required great improvements. The latter half of the 20th century was revolutionary for ultra precision machining. The 60s was were it first kicked off with simple on axis, rotationally symmetric optics [9]. In the late 70's off axis parabolas were being cut on a state of the art diamond turning machine at Lawrence Livermore national lab (LLNL) [10]. By the early 80s, the Large Optic Diamond Turning Machine (LODTM) was built at LLNL, providing the most accurate large optical surfaces that had been produced up to that time. [11]. Since then, ultra precision machining has grown and is used to create everyday items like cellphone camera lens and heads up displays to very complicated space telescopes [12]. In the past couple of years, heads up displays and augmented reality have been on the rise and they incorporate complicated multi-sided optical prisms and arrays which were uncommon until now [13].

1.2 Motivation

True freeform optical surfaces that were used in imaging systems can be traced back to the Polaroid SX-70 camera [14, 15]. Since then, freeform surfaces have grown in popularity with optical designers. A freeform surface is defined as "An Optical Surface that leverages a third independent axis during the creation process to create an optical surface with as-designed nonsymmetric features" [14]. There are two key phases in this definition, nonsymetric features and third independent axis. This definition was build upon the creation of rotationally nonsymetric polynomial aspheres which was brought to life with the development of the slow servo system. The slow servo system allows the machinist to precisely coordinate and time the motions of the linear axis with the rotation of the main spindle [16]. Ultra precision manufacturing machines have been around for manufacturing optics since the early 50s with the creation of a three axis computer numerical control (CNC) by the Moore Special Tool Company [17]. As the design of and desire to create freeform optical systems grew, the ultra precision machinery also developed to accommodate. The addition of a coordinated slow servo and was a game changer for freeforms but it was a slow process due to the limited mechanical bandwidth of the system. As a response to increased production rates of freeform system, the fast tool servo was created to decrease manufacturing time but at the cost optical sag capabilities [18, 19]. More and more complex large sag freeform systems were being designed where turning was no longer a feasible manufacturing method. This brought to life the ultra precision high speed milling spindle. The milling configuration allows the creation of optical surfaces that are not rotational in nature [20]. It also allows for the manufacturing of systems with hard to reach areas and steep slopes that would exceed the capability of a turning operations [18]. The addition of other axis like the A and B axis allow the machine to keep the tool normal to the surface of a part which would reduce error contributions from the tool geometry and waviness [21].

1.3 Challenges of Multi-sided Optics

Multi sided optical systems are being actively designed and used in many augmented reality, virtual reality, heads up displays, and head worn displays. Bauer explains how freeform surfaces on multi sided systems can be used to create high quality head worn displays like the system shown in Figure 1.1 [13].

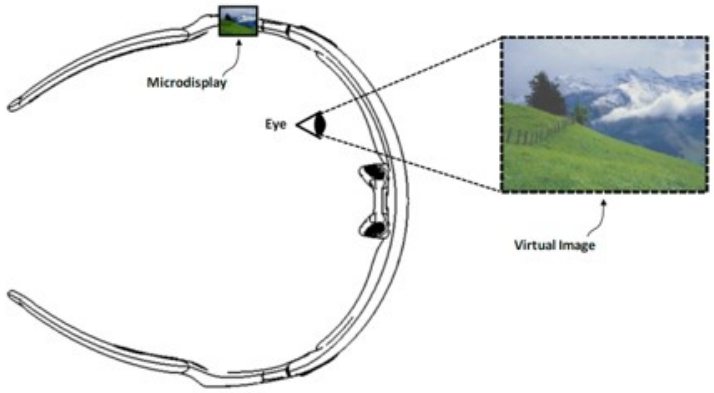

Figure 1.1: Head worn display.

Freeforms are important to these systems because they are less sensitive to alignment errors, they can provide a larger field of view, they can reduce the size of the optical system, and there is a performance increase. Kiontke shows the use of a multi-surface freeform element in an infrared camera (Figure 1.2) that was created to reduce sensitivity to assembly errors [22].

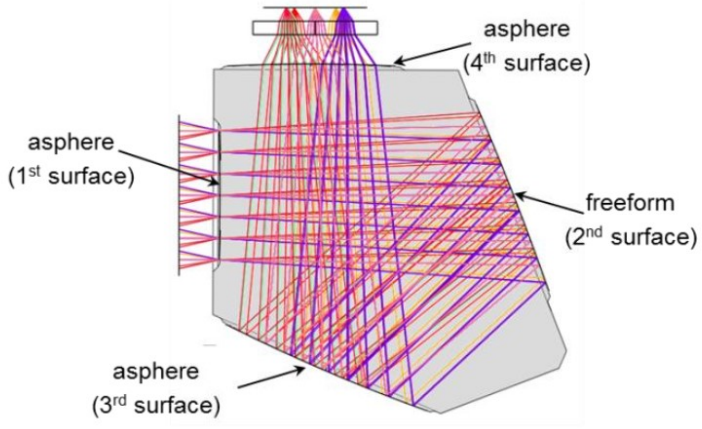

Figure 1.2: Multi-surface freeform element.

Monolithic systems are important when alignment of surfaces is difficult or not feasible. Multi-lens optical systems used in heads up displays and VR are small which creates problems when trying to align and mount multiple surfaces. Transitioning multi-lens systems to monolithic systems allow for reduced assembly errors and reduce the time required to set up the system [23]. The alignment and tolerances of the surfaces in a monolithic system are determined by the errors of the manufacturing machines and process. Kinematic features or other reference features can be cut relative to the optical surfaces in the same manufacturing set up to reduce fixturing uncertainty. These monolithic multi-sided freeform systems are becoming more and more popular in design but little has been published regarding the technical manufacturing of such systems.

Arrays and multi-sided optics have been manufactured in the past but the manufacturing process was very complicated. Barkman et al manufactured a mulit-sided array system in germanium using on-center diamond turning. The system started as a wafer with a gold datum grid. The grid was used as the positioning reference for the system, located with an on-machine microscope. The wafer was positioned using the grid, a lens surface was turned, and then the system was moved to the next lens location. Once one side was completed, the system was flipped and the gold lines were

again referenced using the on-machine microscope. The second side lenses were then manufactured with the same methodology as the first side [24]. The key part of this project is the ability to have a reference feature on both sides of the optical system or substrate. A major difficulty encountered in this specific example is that there was no way of telling how good the reference features were from front to back. A second was time-of-manufacturing and thus cost. Systems that do not have alignment features on the substrate require a method of manufacturing that ensures surface alignment to within a specified tolerance. Each optical surface must have datums to enable manufacturing, metrology, and testing.

1.4 Prototyping Materials

There are many options when it comes to materials that transmit in the visible spectrum. The visible spectrum is any wavelength that is in between 380 to 740 nm [25]. There are two main types of materials that transmit in the visable spectrum. The first is glass or crystal. This includes, N-BK7, UV fused silica, IR grade fused cilica, sapphire, calicum floridem, magnesium flouride, zinc sulfide, zinc selenide, and many others [26]. The second type are polymers, which includes polycarbonate, acrylic, polyethylene terephthalate (PET), allyl diglycol carbonate (ADC), polystyrene, silicone, and many more [27]. Both glass, crystal, and polymer based materials have their pros and cons. Glass and crystal materials have better optical qualities. They also have a higher resistance to scratching and damage. Polymers on the other hand are easy to scratch without protective coatings and are more thermally sensitive than glass and crystal based materials. When it comes to prototype manufacturing, glass can be used for small systems with a low amount of sag (sag $<$ 5 mm) that can be ground and polished without too much trouble. Glass like materials become a problem when the design is large and contains a large amount of sag that requires near net roughing prior to cutting on the ultra-precision machines. Polymers are much easier to machine large amounts of material to get the optic to a near net shape. Tool

wear is also considerably less in the ultra-precision machining of polymers than with glass or crystal materials. For the target application of this work, polycarbonate was chosen because it is light weight, easy to machine, and has better optical qualities when compared to other polymers with similar density [28].

1.5 Thesis Goal

The goal of the work presented in this thesis is to develop a methodology for the manufacturing of complex multi-sided optical systems. Many different multi-sided systems have been designed, fabricated, and tested but there is little to no information about how they were manufactured and how the surfaces are referenced to each other. Ultra-precision manufacturing is no easy task as it is, let alone when the system has to be taken down and re-fixtured to manufacture sequential surfaces. This thesis outlines the steps taken to manufacture such a system. The methodology is intended to be general, and can be used directly as a set of instructions for others manufacturing similar systems, or as a solid starting point for other systems that require re-fixturing.

CHAPTER 2: Experimental Arrangement and Procedures

2.1 Equipment

Two CNC 3 axis mills and an ultra-precision diamond turning machine were used in the manufacturing of the multi sided demonstrator. A 3 axis Haas tool room mill, Figure 2.1 was used for milling the iteration one optical assembly near net. It was also used to manufacture the vacuum chuck and the optical fixturing for the second iteration. A 3 axis Haas office mill, Figure 2.2 was used for the near net of the second iteration demonstrator. The office mill was used over the tool room mill because of its high spindle speeds which allowed for faster cycle times [1].

Figure 2.1: Haas tool room mill.

Figure 2.2: Haas office mill. [1]

A Moore Nanotech 350FG, Figure 2.3 was used for the testing of cutting parameters, the testing of coolant/lubricants, and for the manufacturing of the multi-sided free form demonstrators for both iteration one and iteration two. The 350FG is a five axis ultra-precision diamond turning, diamond milling, and grinding machine which was specifically designed to cut free form surfaces. It has three linear axis', a C axis spindle, and a removable B axis. Iteration one and iteration two utilized the three linear axis', the C axis, and a high speed ultra-precision milling spindle. Parts are held to the C axis using a vacuum system, where custom vacuum chucks can be manufactured to hold the part. The 350FG is equipped with a digital indicator that can be used to center and align parts on the chuck, milling tools, and various other fixturing.

Figure 2.3: Moore Nanotech 350FG

A Sigma Electronics SB-8002 field balancer was used to balance the high speed milling spindle. The balancer uses a magnetic accelerometer that mounts to the side of the spindle and a tachometer to find where the system is out of balance and how to correct it. This system is shown in Figure 2.4.

Figure 2.4: Sigma SB-8002 field balancer.

2.1.1 Metrology

Four pieces of metrology equipment was used during the course of this project. Two scanning white light interferometers (SWLI) were used to evaluate the surface roughness and waviness of the optical surfaces. The Zygo Zegage plus, Figure 2.5 was the first system used.

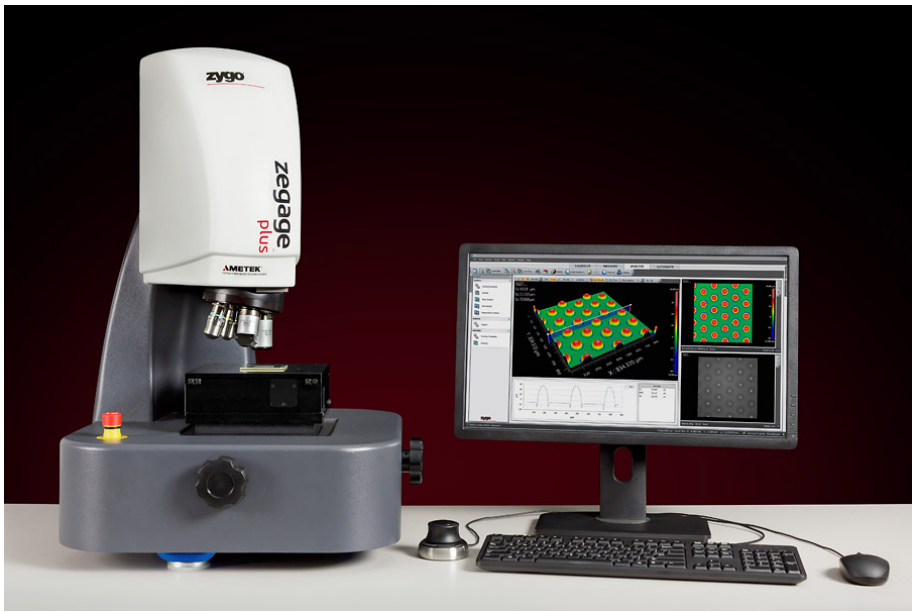

Figure 2.5: Zegage plus SWLI. [2]

It is equipped with three objectives, a 5x Michelson, a 20x mirau, and a 50x mirau. This system is capable of sub-nanometer vertical resolution and 330 nm spatial resolution. The second SWLI was the Zygo Nexview which features similar capability as the Zegage plus but with better vibration isolation and automation. The remaining two metrology systems are used primarily for waviness and form measurements. The first was the Taylor Hobson Talysurf profilometer which has 12.8nm of vertical resolution [29].

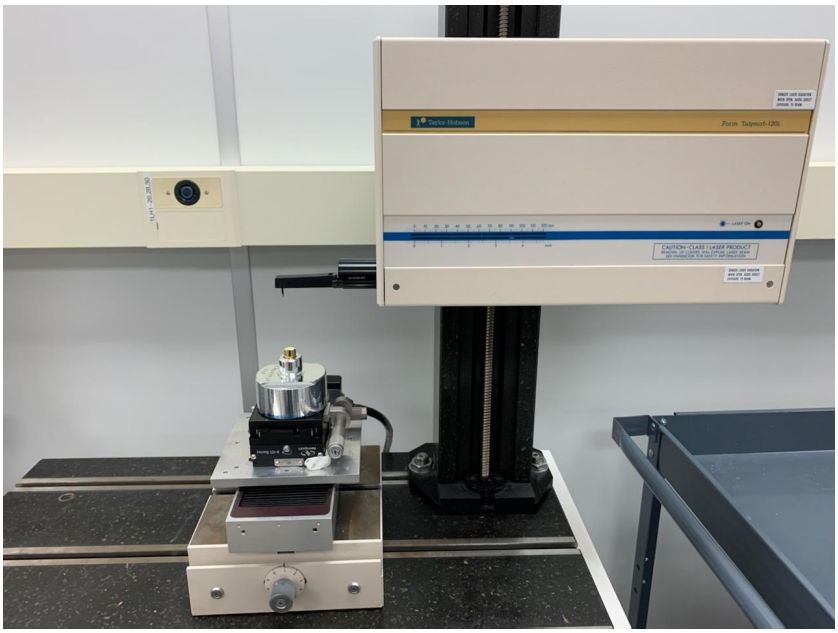

Figure 2.6: Taylor hobson form talysurf.

The talysurfs' primary role in this research was to assist with form measurements of a sphere when setting up a tool. The last metrology instrument was the work error compensation system (WEC) which was also used for setting up a tool. The WEC is a linear variable differential transformer (LVDT) which measures linear displacement after contacting a surface with its ruby tip. The WEC is used to measure spheres for tool correction and to create correction profiles for complex rotational surfaces. A reference master ball is first measured to create a correction profile for the ruby tip. Once the ruby tip is mapped, measurements of surfaces can be made.

2.2 Software

2.2.1 Zemax

The first main software used was the optical design software, Zemax. The Zemax optical design software was launched in 1990 to assist engineers and scientists in bringing ideas to life at a faster and more efficient path . It is a powerful system that enables the design, optimization, and visualization of optical surfaces and assemblies [30]. In this project it was primarily used by the optical designer to design and

optimize the system. Once that was complete, the ray traces, drawings, 3D models, and prescriptions were exported for use in the manufacturing process.

2.2.2 MATLAB

MATLAB is a highly capable data processing and analysis programming language and software. It is capable of data analysis, graphics, programming, app building, external language interfacing, hardware interfacing, parallel computing, web and desktop deployment, cloud based environments, and much more [31]. MATLAB's primary function in this project was for the validation and generation of the optical surfaces for use in NanoCAM.

2.2.3 SOLIDWORKS

SOLIDWORKS is a comprehensive 3D design platform that helps users to conceptualize, create, validate, communicate, manage, and transform ideas to designs [32]. In this project, SOLIDWORKS was used for the designing of the optical fixturing and the diamond turning vacuum chuck.

2.2.4 MasterCAM

MasterCAM is an advanced CAD (computer aided design)/ CAM (computer aided manufacturing) software platform. This software allows users to load in 3D models and assign manufacturing methods to features on the model [33]. The manufacturing methods are fully customizable for just about any tool option or model feature. Once the tool paths are generated from the manufacturing method, they are exported to the machine for manufacturing of the physical part.

2.2.5 NanoCAM4

NanoCAM4 is an opticlly precise ultra-precision CAM software that is specifically design to optimise the manufacturing of optical surfaces on Nanotech ultra-precision manufacturing centers. This software is capable of programming up to 6 axes of simultaneous motion with unparalleled precision [34]. In this project, the 3 axis

capability was used for the milling operations. Once the model and surfaces are loaded into NanoCAM, the surfaces can be compared to surfaces in the model to ensure correct placement. The manufacturing methods and tool geometry are selected, then the tool paths are customized and processed. The processed code is uploaded to the manufacturing center where optical surfaces are manufactured.

2.3 Diamond Turning and Diamond Milling Operations

2.3.1 Diamond Turning

Classical turning operations involve the removal of material from a workpiece by rotating the work piece and moving a stationary turning tool into it to create the desired shape. Turning tool cutting edges vary from high speed steel to diamond. In ultra precision applications, like optics manufacturing, controlled waviness edge single crystal diamond tools are used. Figure 2.7 shows an example of an ultra precision diamond turning tool.

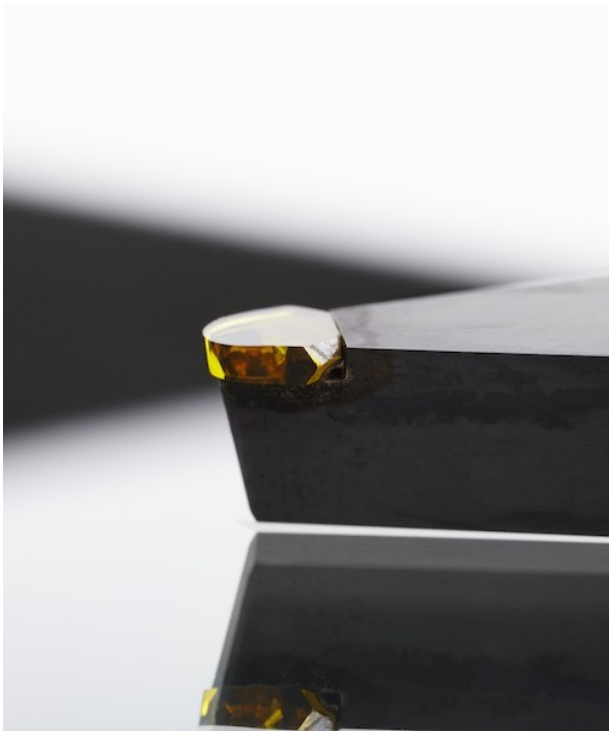

Figure 2.7: Ultra precision diamond turning tool.

The turning operation involves multiple critical parameters. The six main parameters are spindle speed, in-feed, surface speed, depth of cut, tool radius, and tool rake angle. Spindle speed is the rotational rate of speed of the work piece and is typically in the units of revolutions per minute (RPM). In-feed is the rate at which the tool is moving along the surface. In-feed is sometime called feed rate and is measured in units of length per time or length per rotation of the spindle. Surface speed is the rate a which the surface of the part is moving past the cutting edge. It is calculated by multiplying the spindle speed by the circumference of the part at the cutting location. Figure 2.8 illustrates the major parameters.

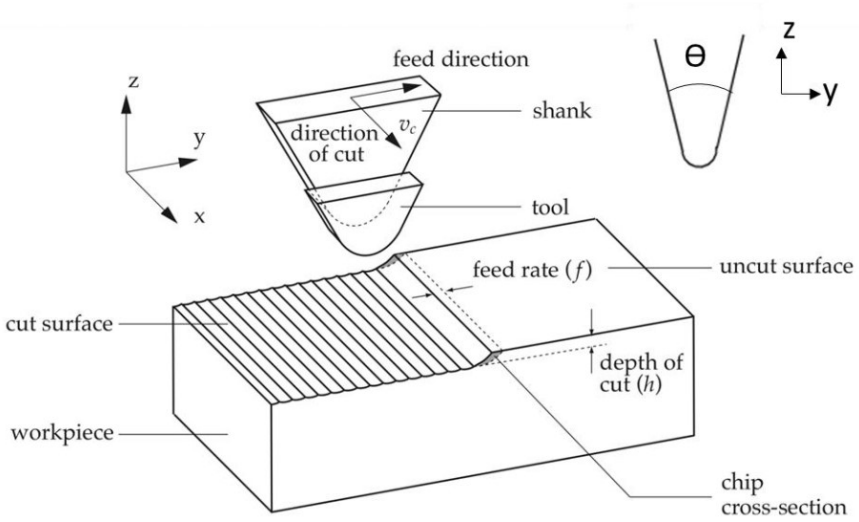

Figure 2.8: Turning geometry and terminology. [3]

The tool radius defines the shape of the structure that gets cut into the part. It also defines the in-feed rate, the larger the radius the larger you can feed per revolution of the spindle and maintain good surface roughness. The rake angle of the tool is how the top face of the tool is angled relative to the horizontal plane. A negative rake is used for brittle materials and a zero or positive rake is used for ductile materials [3, 24, 35]. The tool geometry is shown in Figure 2.9.

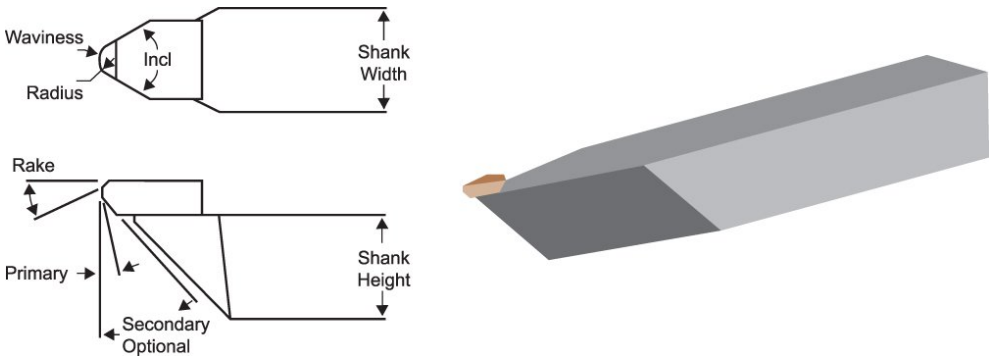

Figure 2.9: Ultra precision diamond turning tool geometry. [4]

2.3.2 High Speed Diamond Milling

A milling operation involves the use of a rotating tool. The rotating tool removes material from the work piece in the form of small chips. There are two forms of milling. The first is conventional or up milling and the second is climb or down milling. The two types are shown in Figure 2.10.

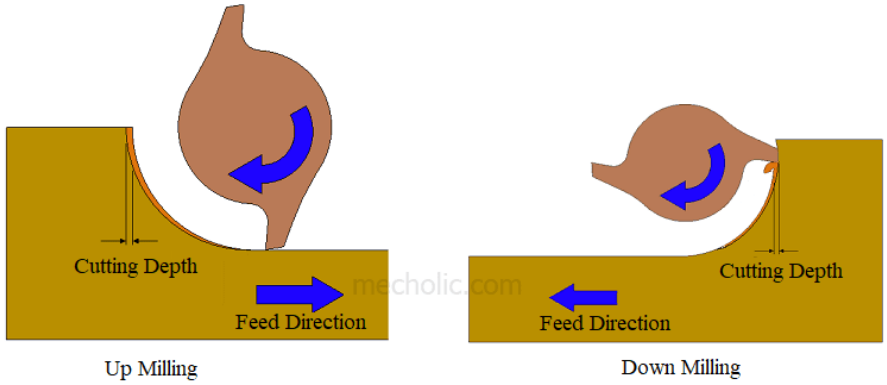

Figure 2.10: Conventional and climb milling operations. [5]

There are many different types of milling tools as shown in Figure 2.11. This project utilizes the sphere and bull nose mill type.

Figure 2.11: Common mill types. [6]

Milling operations also have critical parameters and some relate to turning operations. In milling, feed rate is in the direction of the cut. Spindle speed is not the rotational rate of the workpiece as in turning but is the rotation rate of the tool. Chip load is the ratio of feed rate to spindle speed. It determines the advancement of the tool per revolution and is therefore critical in finding the uncut chip dimensions. For low chip load for an end milling with a radius, step over is comparable to in feed per revolution in turning. Both determine the dimensions of the cusp pattern that dominates the surface and thus relate to geometric surface roughness parameters. The axial depth of cut is the infeed of the tool perpendicular to its rotation axis between passes over a surface. A diamond milling tool can also have different rake angles and geometry that effect the cutting process.

2.4 Machine Setup

The work completed in this thesis used a straight on micro-milling set up, Figure 2.12.

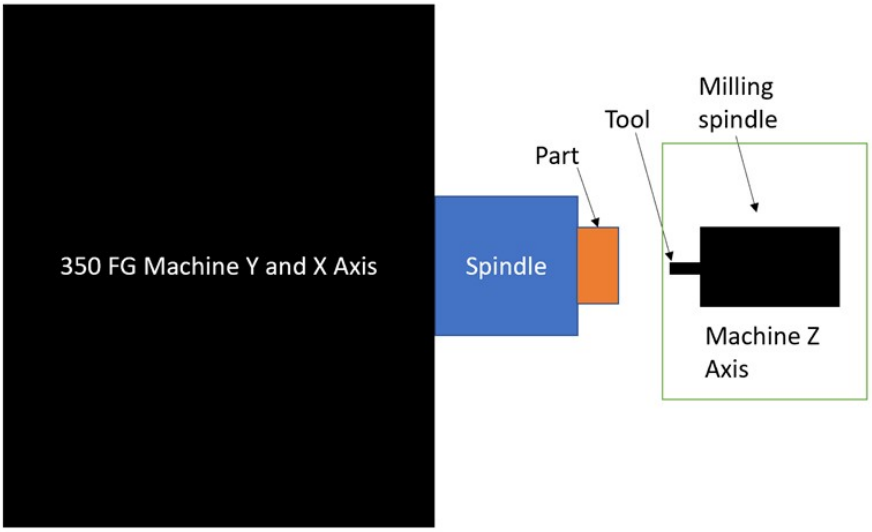

Figure 2.12: Milling configuration.

The mill spindle was oriented perpendicular to the face of the C axis work spindle. A turning tool was also set up next to the milling spindle. The milling spindle is mounted to the Z axis of the machine and the spindle moves in the X and Y direction as shown in Figure 2.13.

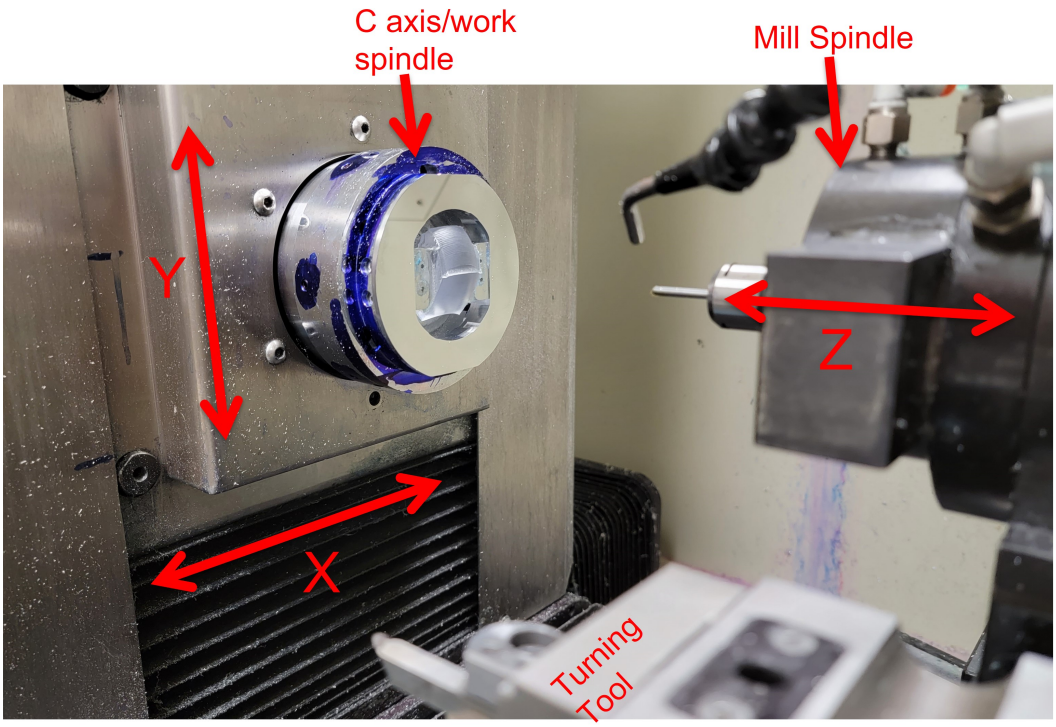

Figure 2.13: Milling configuration and axis motion.

2.5 Milling Tool Set Up Procedures

For the purposes of this research diamond sphere mills (ball mills) were used to cut the optical surfaces of the test patches and the demonstrator. As with diamond turning operations, the milling tool set up is just as critical and is somewhat more complex.

2.5.1 Tool and Spindle Setup Procedures

1. Select the spindle collet required for the diamond mill shank.

2. Install the collet and diamond mill into the spindle.

3. Center the tool in the collet adapter using the digital height indicator and hand tighten the collet adapter mount screws.

4. Using the optical tool setter and orient the tool such that the table is facing

up, find the edge of the tool at the furthest point away from the center line and save the machine X location.

5. Rotate the tool 180 degrees such that the tool table is facing down and jog the machine X such that the OTS is lined up with the edge of the tool. Note the machine X location.

6. Take the average of the two machine x locations and move the machine to that location in x and move the machine Z such that the tool tip is in view.

7. Rotate the tool so that the table is facing upwards and check that the diamond becomes tangent with the OTS X axis reference position. If it does not, find a tool that does and get the one that doesn't fixed.

8. Tap the collet adaptor until the tangent point of the tool is as close as possible to the rotational center line of the mill that was found earlier. Ensure it is at the center line or away from the rational center line and not past the rotational center line.

9. Rotate the tool and check alignment of the tool table to the rotational center line

10. Tap the table towards the rotational center line as close as possible

11. Rotate back to the table facing upward and check the tangent point. Tap in as needed

12. Tighten the collet adaptor mount screws and verify nothing shifted.

    (a) A tool that crosses the rotational center line is called an inverted bull nose mill and is not correctable in CAM software.

    (b) A tool that is away from the rotational center line is called a bull nose mill and its correctable if it reaches a tangent point.

(c) Figure 2.14 shows the possible milling tool configurations. Figure 2.14(a) is a diamond that is past the rotational center line and does not reach a tangent point with the horizontal axis. Figure 2.14(b) is a diamond that is at the rotational center line but does not reach a tangent point with the horizontal axis. (a) and (b) are not correctable. Figure 2.14(c) is a diamond that reaches a tangent point and is at the rotational center line. This is an example of an ideal ball mill. Figure 2.14(d) is a diamond that reaches a tangent point but needs to be tapped towards the rotational center line such that it becomes less of a bull nose mill. Figure 2.14(e) shows a tool like (d) but that needs to be tapped the other direction to become a bull nose mill. 2.14(f) is another example of an ideal ball mill.

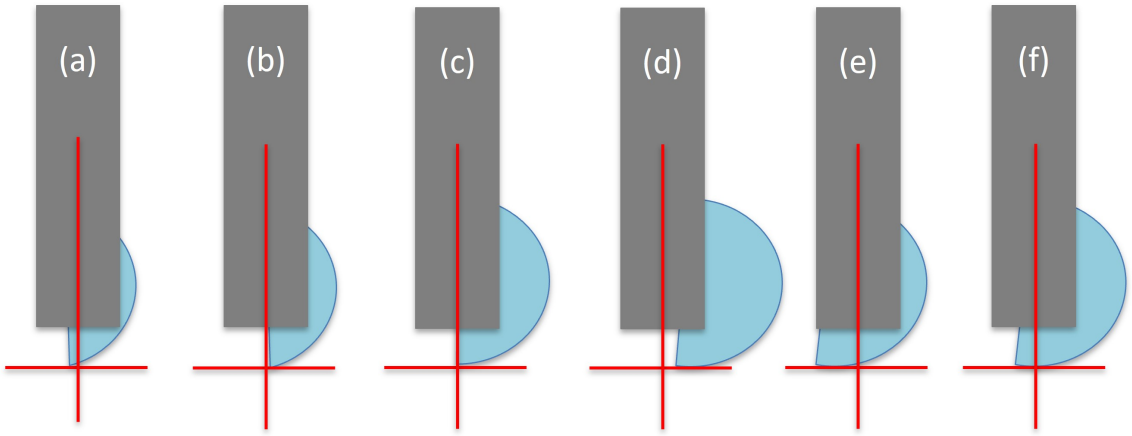

Figure 2.14: Examples of good and bad milling tools.

13. The final step to a tool setup is to balance it using a high speed spindle balancing system like the Sigma Electronics SB-8002 field balancer. Start at low RPM and work up to the operating RPM. The high speed spindle was balanced to a 5 nm amplitude of oscillation (as reported by the balancer) at 40,000 RPM for the work completed in this research.

2.5.2 Tool Centering and Geometry Characterization

Tool centering involves finding the location of the tools rotational center line relative to the main work spindles rotational center line. This is most critical when the C axis is used in the milling operation as for an X,Y,Z raster milling operation, the offset is not seen,The following steps guide the process of centering a milling tool.

1. Fabricate a centering pin as shown in Figure 2.15.

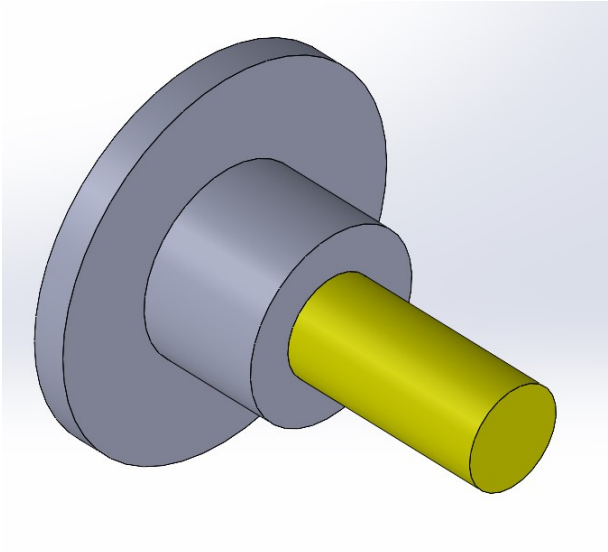

Figure 2.15: Start of the milling tool centering stud blank.

2. Center the pin on the main work spindle and diamond turn a 45 degree chamfer. The chamfer is now concentric to the work spindle center line. See Figure 2.16

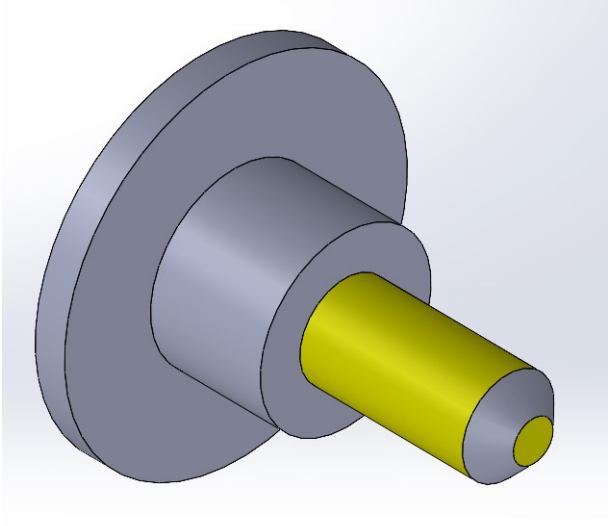

Figure 2.16: Milling tool centering stud with diamond turned chamfer.

3. For centering in the x direction, move the tool to the nominal Y 0.0 location and with the milling spindle on and the work spindle at an rpm of five or less, touch off the side of the 45 degree chamfer to create a band as shown in Figure 2.17. Store the Z and X location of the tool when the band is created.

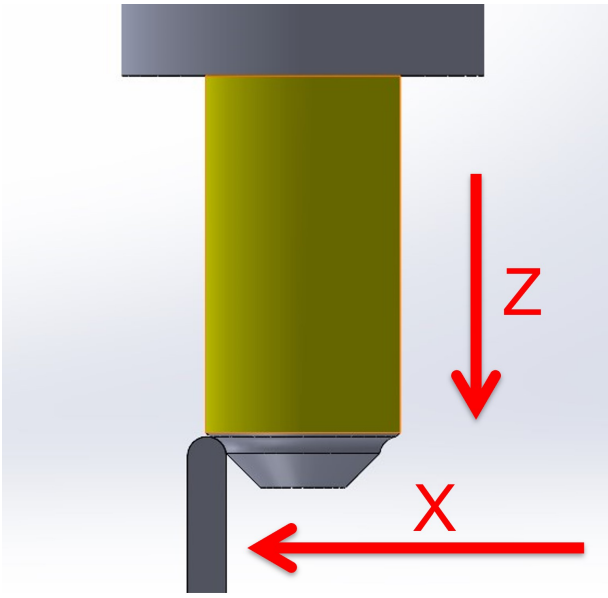

Figure 2.17: Touching off the centering stud to reference left side of stud (machine X).

4. Without changing the Y and Z location, move the X axis in small increments (1 um or less) and touch off the groove from the other side of the pin as shown in Figure 2.18.

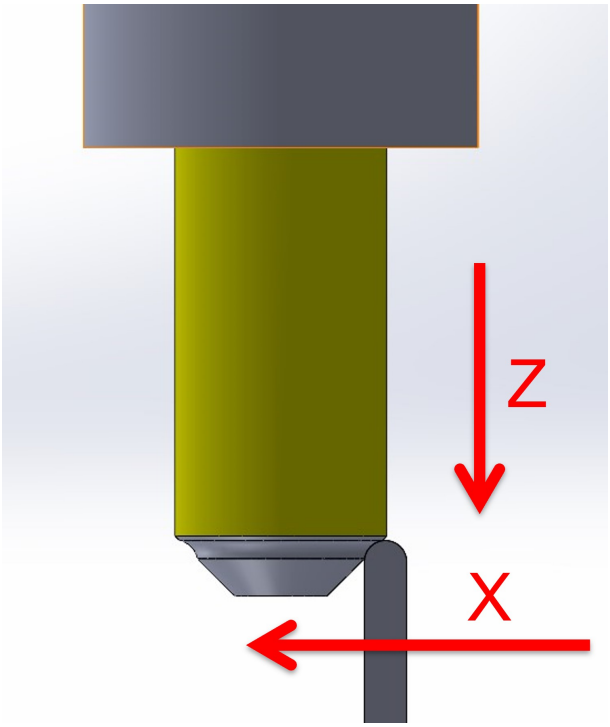

Figure 2.18: Touching off the centering stud to reference right side of stud (machine X).

5. Once you see material being removed, switch to a smaller increment and slowly back away until you are not touching the band anymore. Store that X location.

6. Take the average of the two locations and that will tell you how far off you are in the x direction and the tool can be centered on the C axis to better than the final increment used to slowly move off the part in the previous step.

7. Repeat in the Y direction to center the tool in the Y direction.

8. The tool and work spindle are now aligned.

Now that the tool is centered, the diamond offset from rotational center line and radius can be determined.

1. Using an on center turning tool, turn a concave sphere into the end of the centering pin as shown in Figure 2.19.

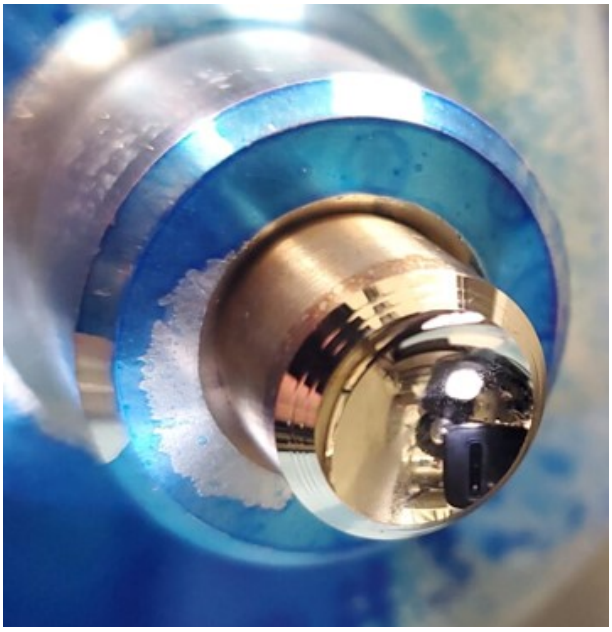

Figure 2.19: Milling tool centering stud.

2. Setup the tool as a spherical milling tool (ball mill) in the CAM software.

3. Using the milling tool raster mill the sphere.

4. Take note of the raster direction.

5. Measure the sphere on a profilometer in the direction of raster.

6. The Moore Nanotechnology manual shows two charts, Figure 2.20, to interpret the profilometer reading once a fit sphere is removed.

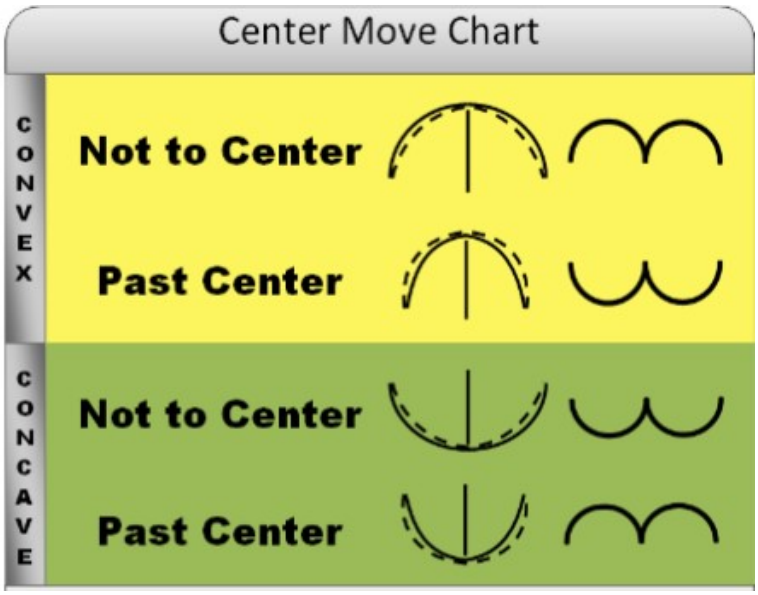

Figure 2.20: Nanotech tool centering chart with errors form best fit sphere in the right most column (error is calculated by subtracting the best fit sphere from the measurement.)

7. When starting from a tool that is modeled as a spherical mill in the CAM and a tool that is set up as a correctable geometry (as shown in Figure 2.14 (d)), it will produce an outcome of "not to center". This error is because the tool motion was programmed based on a spherical tool while the actual tool is a bull nosed endmill.

8. Using the peak to valley value of the W error, calculate the diamond offset. This is an automatic feature in the Nanotech WEC software and NanoCAM.

9. Now model the tool as a bull nose mill with a flat at the tool tip that is twice the center error that was calculated.

10. Reduce or increase the corner radius based on the radius correction found by subtracting the best fit sphere from the theoretical sphere. On a concave sphere, if the value is positive then subtract the difference from the modeled tool radius in the CAM software. If it is negative then add to the modeled tool radius in the CAM software.

11. Repeat this process until the tool radius and offset is correct, a PV error value less than 100 - 200 nm is well corrected

2.6 Importance of Equipment and Procedures

The equipment, metrology, and software presented in this chapter are critical to the work completed in this thesis. Without the equipment and proper knowledge of the system and processes, optical manufacturing will prove unsuccessful. Now that a tool setup procedure has been developed and outlined, we can proceed with the development of the manufacturing procedure of multi-sided optical systems. A tool that is improperly set up will result in unsatisfactory optical surfaces.

CHAPTER 3: Ultra-precision Machining of Polycarbonate

3.1 Background on Machining of polycarbonate

It is difficult to machine surfaces with less than 10 nm Sq in polycarbonate. The material has has a large coefficient of thermal expansion of approximately 70 ppm per °C [36]. To reduce form and waviness errors due to thermal expansion, the environment must be well controlled. Polycarbonate, like other polymers machines quite different than traditional metals used in reflective optics and molds. Surface quality of ultra-precision diamond machined materials is dependent on a wide range of parameters. These include but are not limited to, cutting operation (milling or turning), depth of cut (DOC), spindle speed, federate, tool geometry, material properties, tool wear, vibration, cutting temperatures, coolants/ lubricants, and lab environment conditions [7, 3]. Milling operations are inherently discontinuous cutting operations and typically result is worse surface finish than continuous cutting turning operations [3]. Current literature focuses on turning operations and does not provide significant information on the effect of milling parameters on surface roughness. The following information on cutting parameters relates directly to turning operations and is interpreted for milling operations. A DOC too large can result in tool chatter and decreasing the DOC past a critical point can result in an increase in surface roughness [37]. Spindle speed changes the surface speed of the material which in some materials can have a large effect on the resulting surface finish. Feed rate and stepover of the tool on the surface creates a cusp structure that, when too large or too small, greatly impacts the surface finish. A large step over results in faster cutting operations but increases the surface roughness. A stepover too small can result in tool rubbing which can also increase the surface roughness [3, 38]. Tool rake angle, clearance angle, and

radius all contribute to the quality of the surface finish because they effect the material deformation. The tool geometry changes based on the material properties. A brittle material will likely use a negative rake angle and a ductile material will use a positive rake angle [7, 3, 38]. Material that is prone elastic spring-back will use a tool that includes a large clearance angle to prevent the material from rubbing on the clearance face [3, 39]. Vibrations in the system can cause nano-meter level variations in the tool location and result in a larger surface roughness. In turning operations, chip rub is a large contributor to an increase in surface roughness. A vacuum and air nozzle system are required to prevent polycarbonate chips from rubbing/scratching the freshly cut surface. Coolants and lubricants, when all other parameters held constant, have a large impact on the surface roughness of diamond machined polycarbonate . Low viscosity and highly conductive cutting fluids reduce built up edge, tool wear, and Sq surface roughness [7]. Gubbels showed that in diamond face turning, the depth of cut and surface speed do not significantly influence surface roughness [3]. Feedrate (in particular feed per revolution) is an influential factor that increases the surface roughness as the feed rate is increased. Figure 3.1, shows how the roughness of polycarbonate changes as a function of feed rate [3].

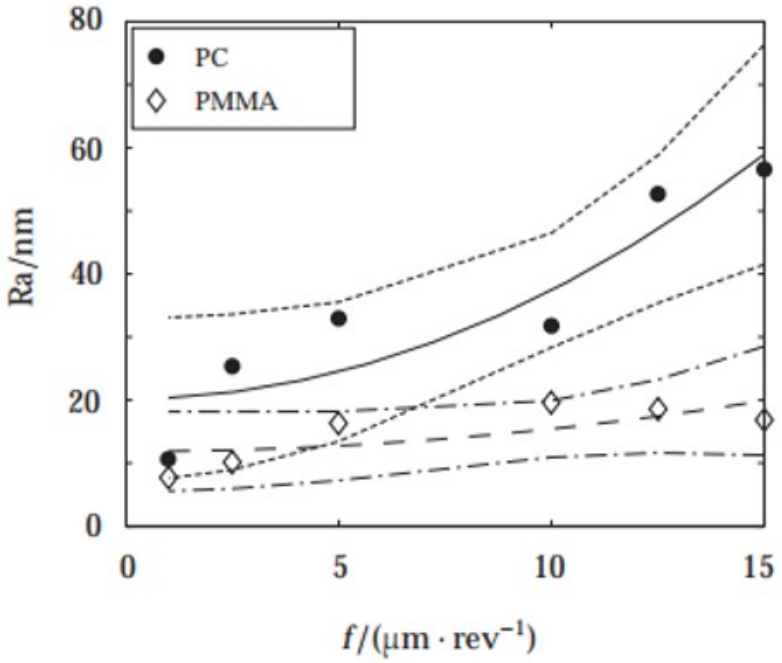

Figure 3.1: Roughness as a function of feed rate. [3]

Bodlapati showed that multiple factors contributed to the surface roughness of diamond turned polycarbonate [7]. In polycarbonate, increasing the feed rate increased the surface roughness which agrees with Gubbels [3, 7]. Boblapati also found that a positive rake tool reduced the surface roughness when compared to a zero rake or a negative rake turning tool. The final major result concerned cutting lubricants. It was concluded in his testing that WD-40, Tap Magic Aqueous, and Kerosene all reduce the surface roughness the most when compared to dry cutting [7]. The results of all the cutting lubricants he tested are shown in Figure 3.2.

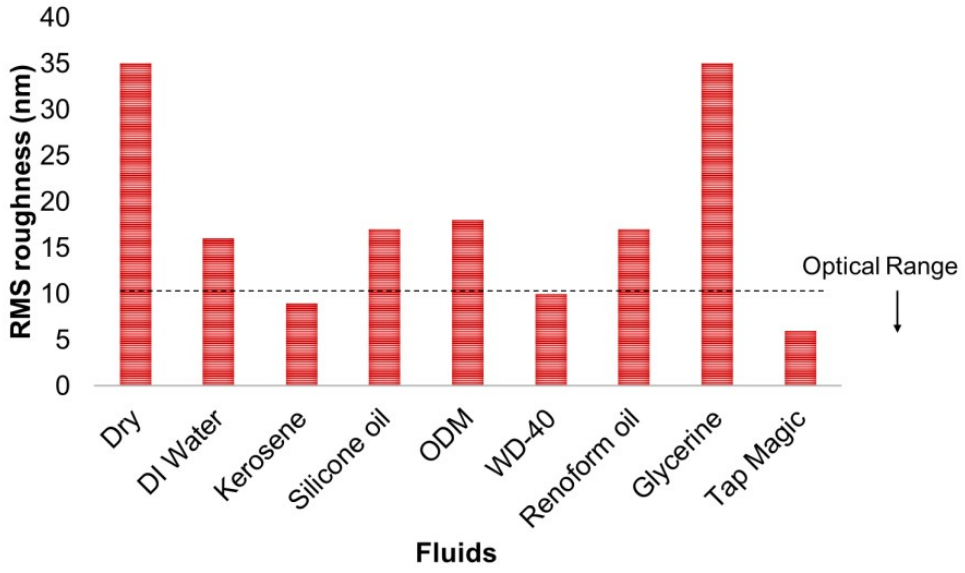

Figure 3.2: Effect of lubricants of surface roughness of diamond turned polycarbonate. [7]

3.2 Testing Optical Surfaces in Polycarbonate

3.2.1 Test Patch Manufacturing

To test the effect of cutting parameters and cutting fluids in milling, a series of test patches on a four-inch polycarbonate disk were created in NanoCAM. Figure 3.3 shows the test patches with their corresponding feed rates and step over. The test was completed on the Moore Nanotechnology Systems 350 FG ultra-precision machining center with a 15 μm DOC.

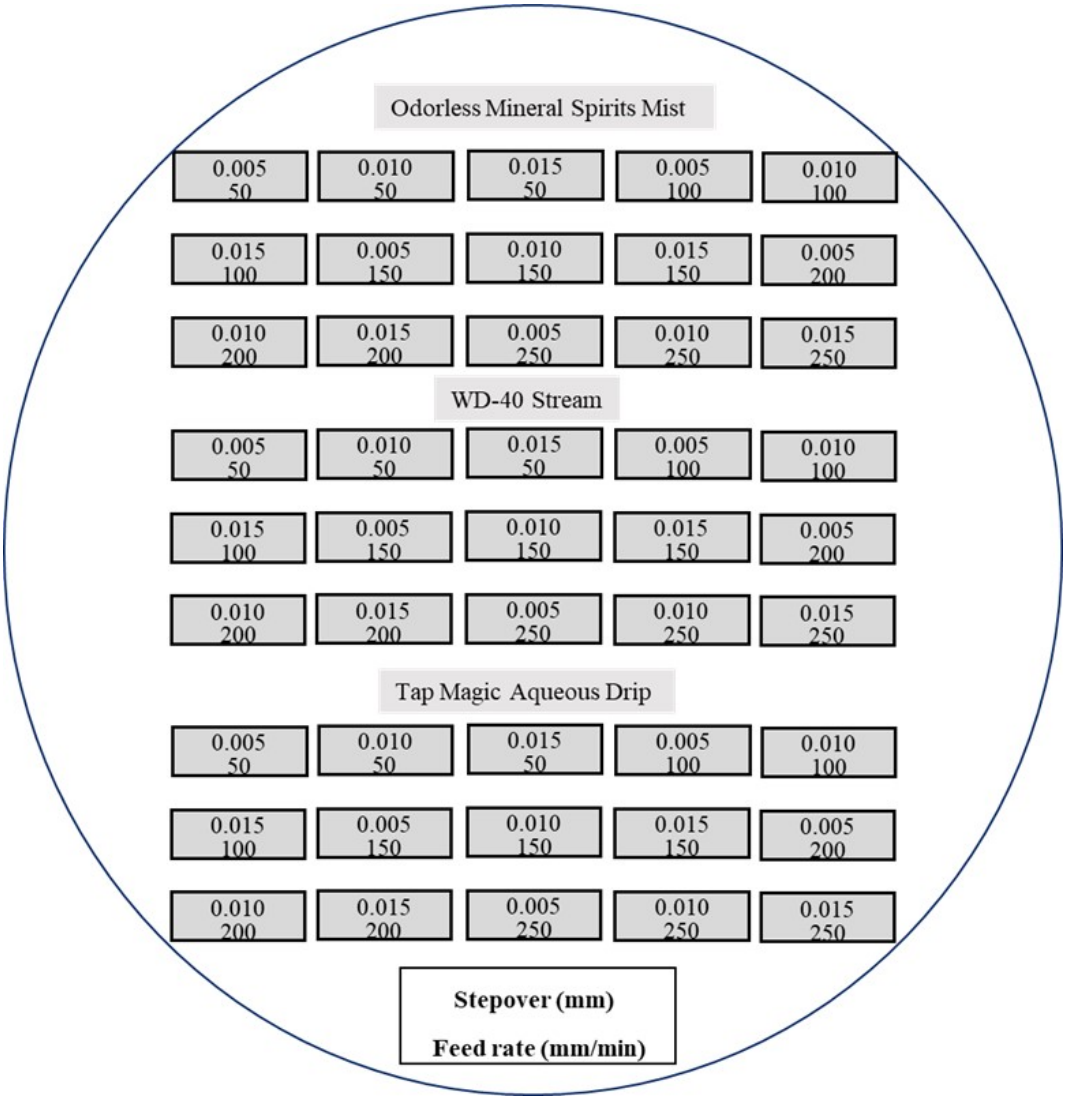

Figure 3.3: Test patches with the corresponding feed rates and step over.

Each set of patches were micro-milled using a 1.8 mm radius sphere mill with the milling spindle perpendicular to the puck surface as shown in Figure 2.12. The spindle speed was 40,000 rpm.

The odourless mineral spirits were applied using an onboard mister, the WD-40 with a recirculation stream, and the Tap Magic Aqueous with a gravity fed dripper. The mister and stream were continuous throughout the cut and the dripper applied the fluid once every second. Once all patches were machined, the polycarbonate puck was placed in an ultrasonic cleaner filled with dawn dish soap and water. The puck

was placed such that the patches were perpendicular to the bottom of the tank. After one hour in the ultrasonic cleaner, the puck was removed and cleaned with water. An air supply was used to spray the water from the puck and test patches.

3.2.2 Test Patch Metrology

Surface measurements of the test patches were made using the Zygo Plus scanning white light interferometer. With averaging set to five, three measurements of each test patch were measured using the 20x objective with 1x zoom.

3.2.3 Data Processing

All data was processed in Mountains maps. Three operations were performed prior to any surface roughness analysis. To remove form, such as piston, tip, and tilt, a first order polynomial was removed from the imported surface. Low wavelength, high frequency surface information was then filtered out using a gaussian s-filter with a cut off (λs) at 2.5 μm. High wavelength, low frequency surface information was then filtered out using a gaussian L-filter with a cut off (λc) of 80.0 μm. Rms slopes parameter required a different band pass filter of 80.0 μm to 2.5 mm. The filtering is in accordance with ISO-10110-8:2019 section 4.3 and ISO25178. Form removal and filtering were required to isolate the roughness of the surface [40]. Figure 3.4 shows a graphical representation of the separation of roughness and waviness in a 2-dimensional profile.

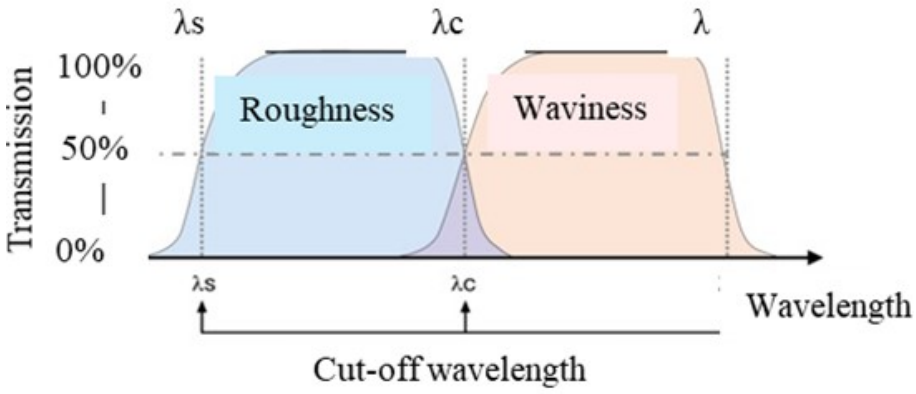

Figure 3.4: Graphical representation of roughness and waviness isolation based on the specified cut-off wavelengths.

3.2.4 Analysis

Once the surface topography was processed and filtered, surface parameters for each measurement were calculated. Surface parameters of the three measurements for each test patch were then averaged together. The results were plotted as a function of feed rate and step over. Yellow represents Tap Magic Aqueous, grey represents WD-40, and orange represents Odourless Mineral Spirits. The theoretical average roughness (Sa) was calculated using Equation 3.1 and is shown in blue in Figure 3.5 [2].

$$Sa = \frac{S^2}{9 * \sqrt{12} * R} \tag{3.1}$$

Where Sa is the average surface roughness,

S is the step over in μm, and

R is the tool radius in μm

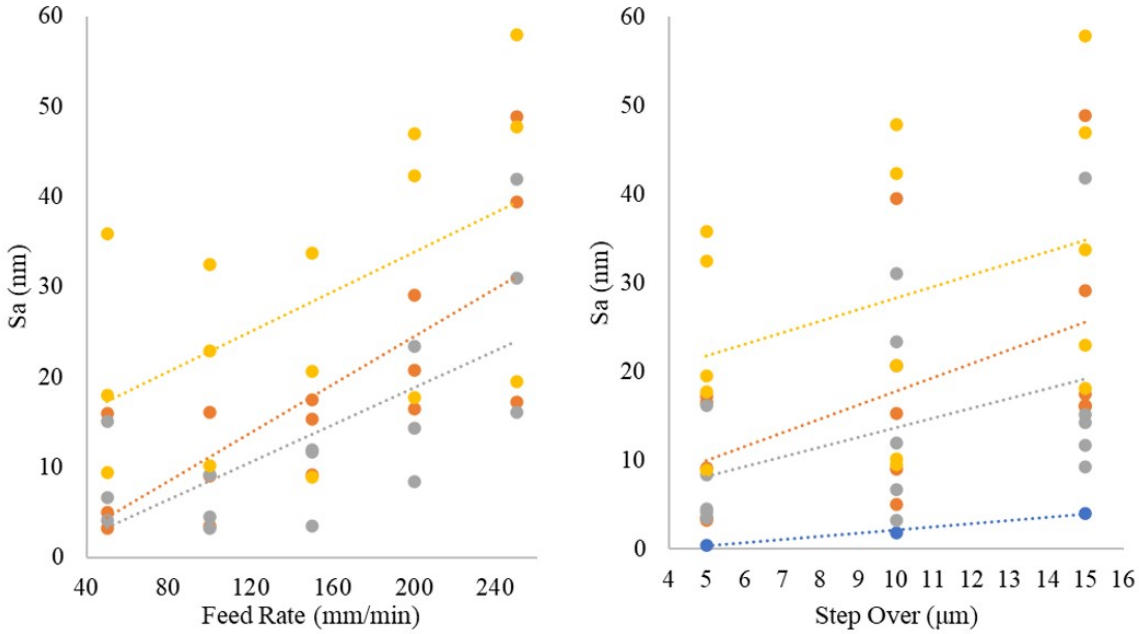

Figure 3.5: Average surface roughness as a function of feed rate and step over. The blue data represents the theoretical average roughness. Grey represents WD-40, orange represents odorless mineral spirits, and yellow represents Tap Magic Aqueous.

The average roughness, Figure 3.5, for each cutting fluid as a function of feed rate and step over show similar trends. The WD-40 with the lowest average roughness, then Odourless Mineral Spirits, and finally Tap Magic Aqueous with the highest average roughness. All cutting fluids showed an increase of average roughness as feed rate and step over increased. WD-40 showed the most similar relationship between step over and average roughness to the theoretical. The theoretical average roughness was formulated for turning operations, but it appears only an offset would be required to predict the roughness of micro milled polycarbonate. A larger sample size would be required to find the offset value. The rms roughness, Figure 3.6, showed the same results as the average roughness with WD-40 performing the best and Tap Magic Aqueous performing the worst.

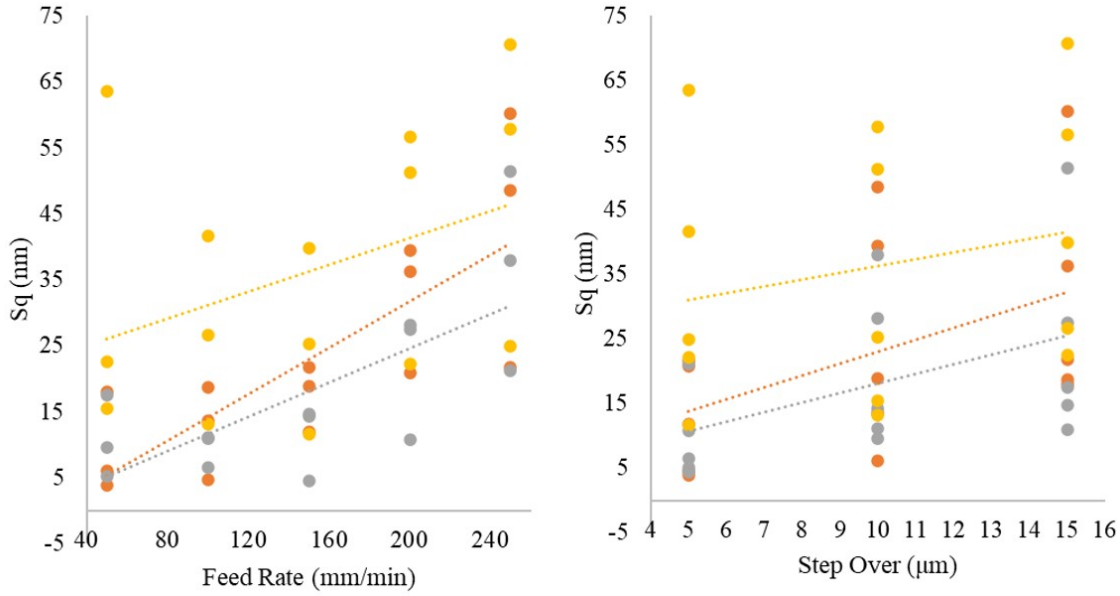

Figure 3.6: RMS surface roughness as a function of feed rate and step over. Grey represents WD-40, orange represents odorless mineral spirits, and yellow represents Tap Magic Aqueous.

The skewness (Ssk), Figure 3.7, showed that as feed rate and step over increased, the peak of the height distribution went from above the mean plane to below the mean plane. Skewness of the WD-40 samples is independent of step over and highly dependent on feed rate when compared to the other cutting fluids.

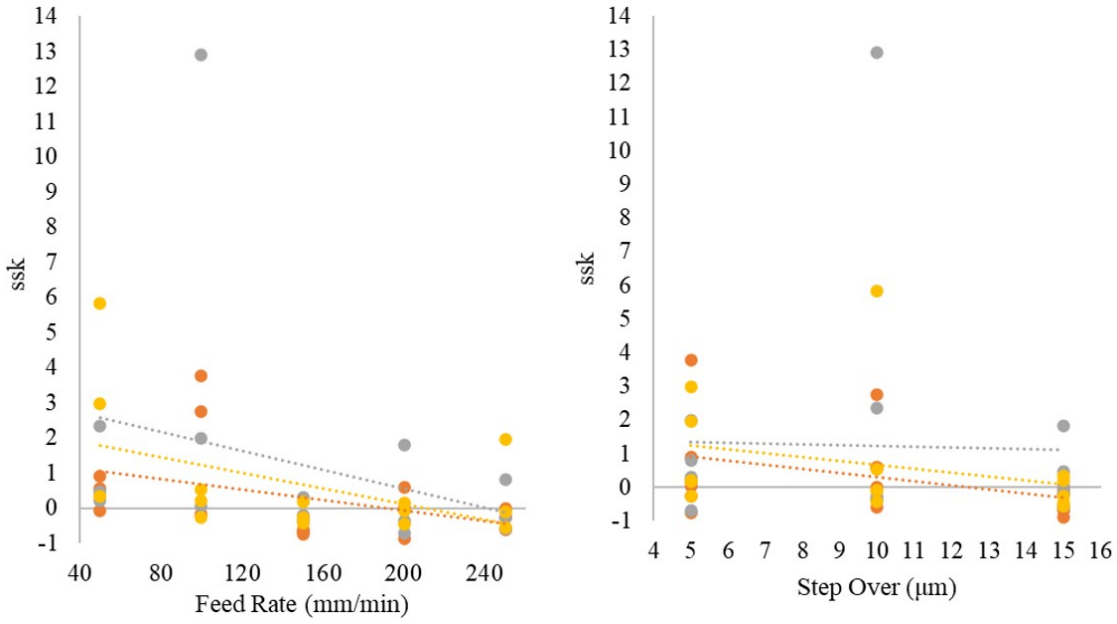

Figure 3.7: Skewness (Ssk) as a function of feed rate and step over. Grey represents WD-40, orange represents odurless mineral spirits, and yellow represents Tap Magic Aqueous.

Kurtosis (Sku) of the surfaces, Figure 3.8, show that the height distributions, Sku larger than 3, are very peaked and not normal. Most of the hight distribution lies close to the mean plane. A smaller Sku indicates that there is a large degree of material pull out, cutting fluid residue, or material adherence on the surface. Sku on the WD-40 surfaces is also independent of the step over and highly dependent on the feed rate when compared to the other surfaces. Tap Magic Aqueous and Odourless Mineral Spirts show that both feed rate and stepover have similar relationships to the Sku of the surface.

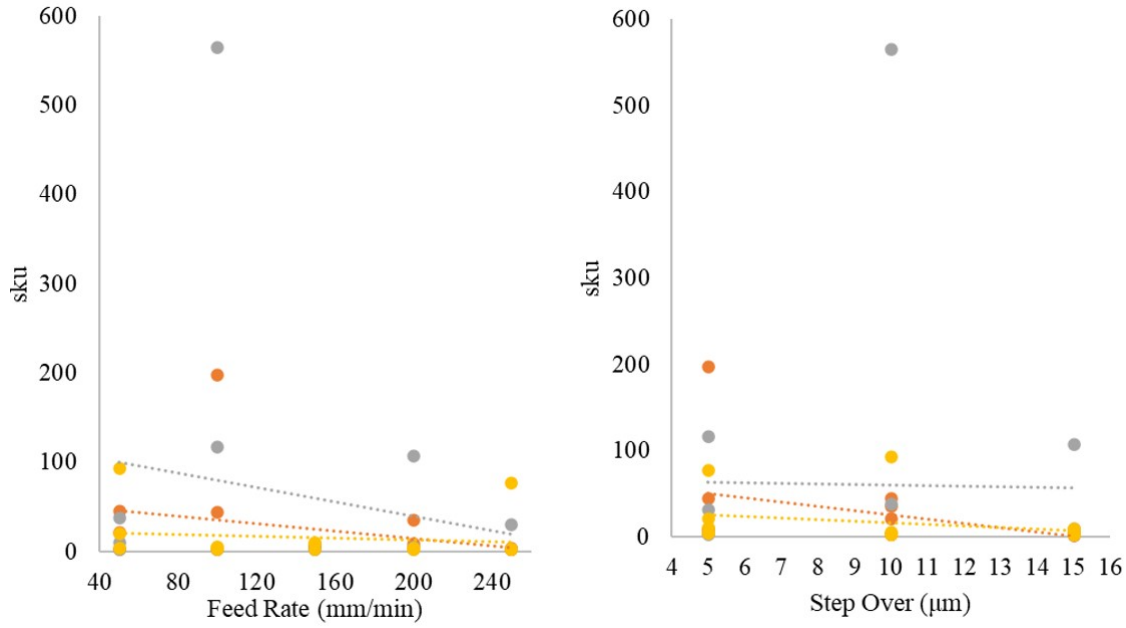

Figure 3.8: Kurtosis (Sku) as a function of feed rate and step over. Grey represents WD-40, orange represents odurless mineral spirits, and yellow represents Tap Magic Aqueous.

The rms slopes, Figure 3.9 can show how much residue and dirt remains on the surface after cleaning. The WD-40 and Odourless Mineral Spirits showed small constant slopes as a function of feed rate and step over indicating that very little residue remained on the surface. Tap Magic Aqueous showed much larger slopes but they are dependent on feed rate and step over. Dependence on feed rate and step over could a result of the fluid dripping and drying onto the upper surfaces while the remaining surfaces were being cut.

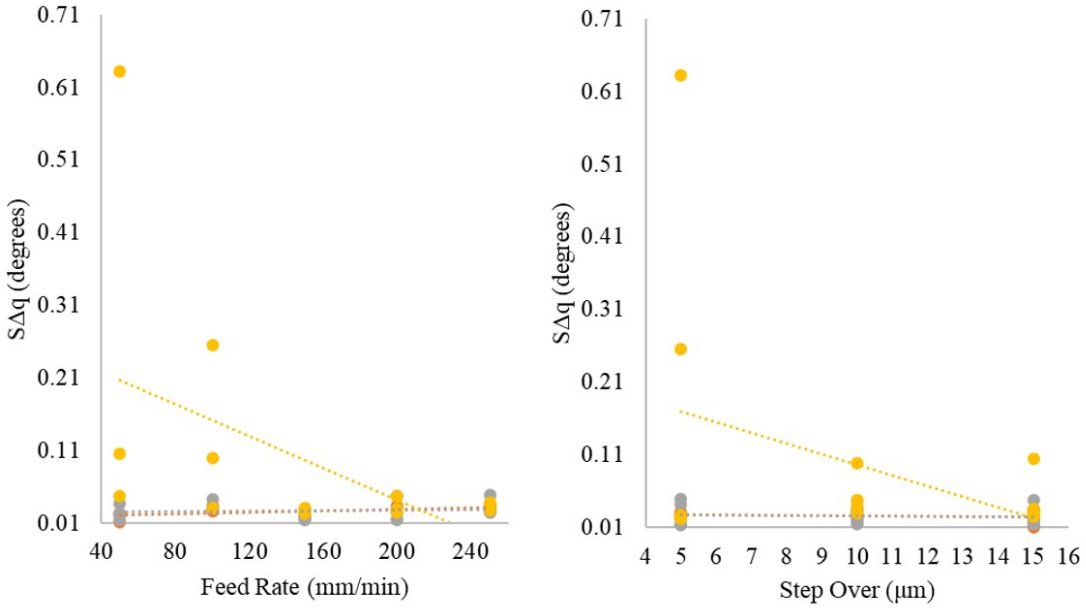

Figure 3.9: RMS surface slopes as a function of feed rate and step over. Grey represents WD-40, orange represents odurless mineral spirits, and yellow represents Tap Magic Aqueous.

Figure 3.10 shows the large amount of material pull out and residue stuck to the surface created with Tap Magic Aqueous, right, when compared to the WD-40 surface, left.

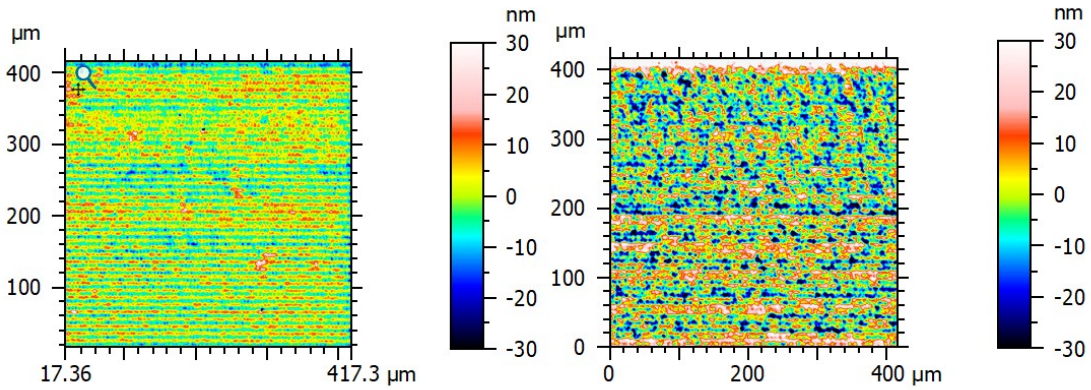

Figure 3.10: Comparison between WD-40 (left) and Tap Magic Aqueous (right) with a 0.010 mm step over and 100 mm/min feed rate.

The images agree with the conclusions that were drawn from the rms slopes, kurtosis, and skewness.

3.3 Polycarbonate Optical Surfaces Conclusion

The purpose of the experiment was to analyse the effect of cutting fluids on the surface roughness of micro-milled polycarbonate. It was found that WD-40 produced the lowest surface roughness and Tap Magic Aqueous produced the largest surface roughness. The roughness did increase as a function of feed rate and step over as expected. Skewness indicated that at high feed rates and step overs, material pull out created many pits in the surface. Kurtosis indicated that the height distribution of the surfaces was very peaked, and they became more normal as the feed rate and step over increased. Step over for the WD-40 had little impact on the skewness and kurtosis while feed rate had a large impact. RMS surface slopes of the surfaces showed that Tap Magic Aqueous, once dried, can be significantly hard to remove from the surface. WD-40 with small feed rates and small step overs result in the best optical quality surfaces with Odourless Mineral Spirits only slightly worse.

CHAPTER 4: Practical Applications

4.1 Iteration 1 - Industry Sponsored Project

Iteration 1 of the multi-sided freeform research was for an accelerated timeline industry sponsored project. The fast timeline did not allow for thorough testing and research prior to the final product. Iteration 1 was the manufacturing of a multi-sided freeform prism made out of polycarbonate. The University of North Carolina at Charlotte has attempted to manufacture similar systems in the past with limited success.

4.1.1 Fixturing

To simplify the process, reduce assembly time, and reduce manufacturing time, a monolithic system was created out of a sheet of polycarbonate, Figure 4.1

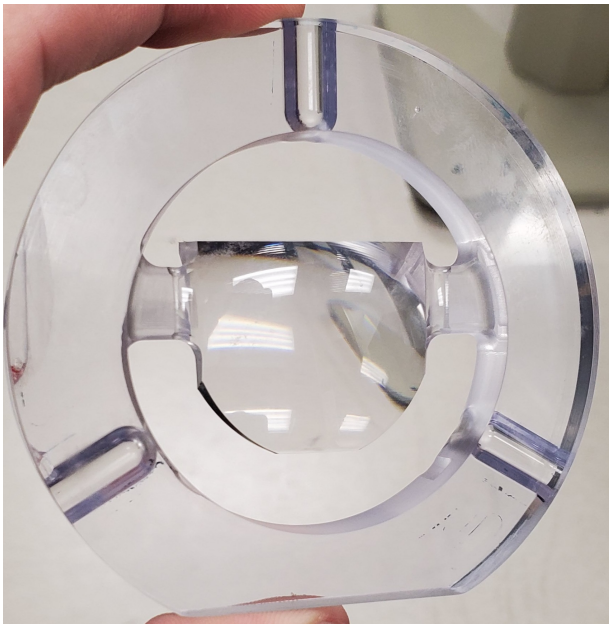

Figure 4.1: Monolithic polycarbonate prism and fixturing.

Using a monolithic fixturing and opto-mechanical ring was a good idea in theory

and would likely have been more successful in a stiffer material. During the manufacturing process of the near net roughing on the non precision Haas toolroom mill, the part was held in a vice. Stresses from the vice caused deformation into a "potato chip" shape. The face was machined flat and when the part was removed from the vice, it relaxed into a a curved shape. Figure 4.2 shows illustrates what happened.

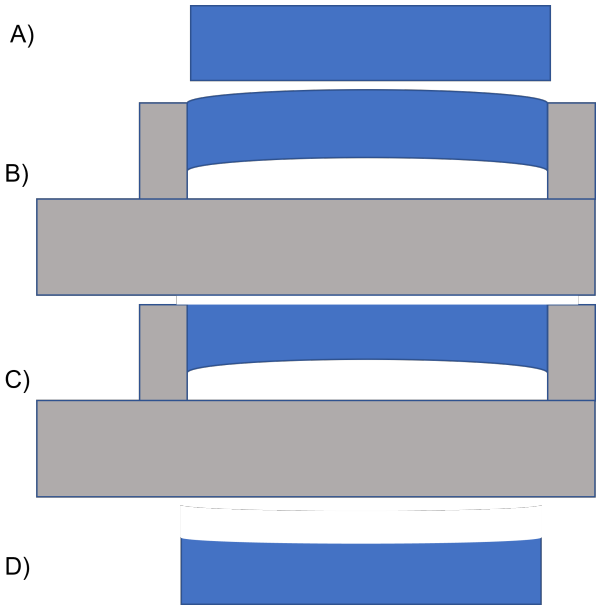

Figure 4.2: Deformation of the fixturing ring during manufacturing.
A) Original Part.
B)Part mounted in the Haas Tool-Room vice deformed
C)Top of the part was machine.
D) Part was removed from the vice and it relaxed to its original shape.

This would not vacuum to the diamond turning machine without deforming the part and thus causing relaxation errors when the part was removed from the vacuum. This phenomenon was noticed during the part set up and corrected by epoxying the part to the chuck with minimal loading. The surfaces where diamond turned flat and made as parallel as possible. Polycarbonate also does not make good reference geometry due to softness and thermally induced deformations.

4.1.2 Cutting Fluid Delivery

The cycle time for the part was long. One surface had a cycle time over 26 hours, and we would have to refill the mist fluid container over four times throughout the cut. This was not ideal as entering the room or adding fluid is not standard practice during the cutting of a finish surface. The fluid would have to be recycled and reused to ensure there is cutting fluid through the cut without any need to refill during the cut. The re-circulation system, illustrated in Figure 4.3, was developed and used for the iteration one optic.

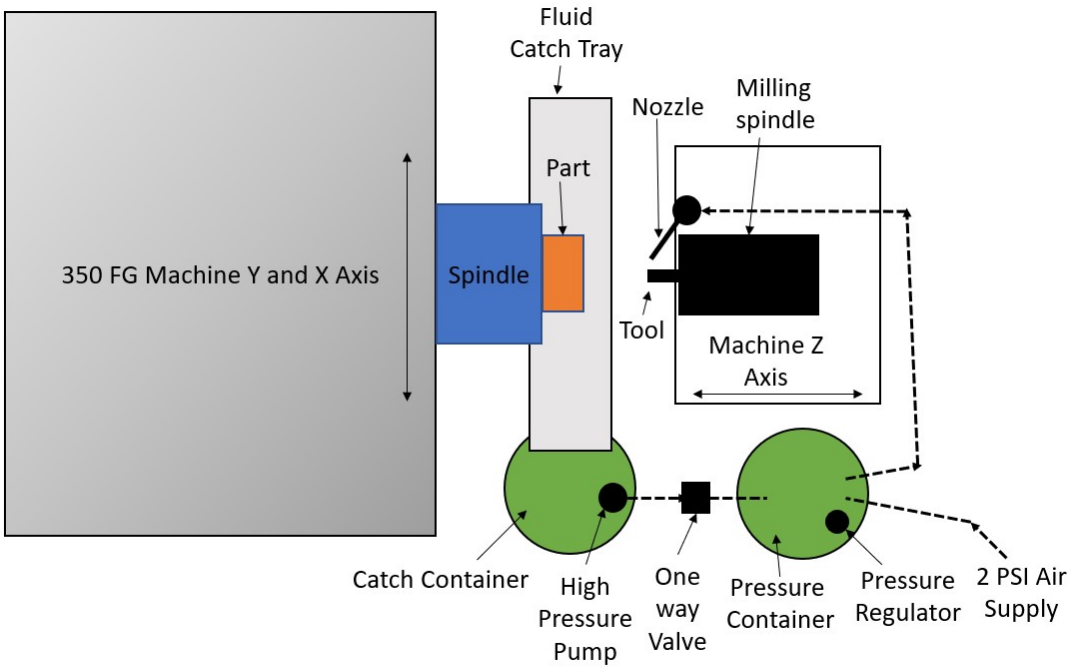

Figure 4.3: Milling coolant system with high pressure pump.

The fluid was pumped from the catch container using a pump that would cut on for a prescribed time every 8.8 minutes. The fluid travelled through a one way valve and into a pressurized container. The container was pressurized using an air supply from the machine and the pressure in the container is regulated using a pressure regulator. The fluid was pushed into the nozzle and sprayed on the part. The fluid ran off the part and into the catch tray and the cycle repeated. This system allowed

the re-circulation of WD-40 for 24 hours before we had to refill due to some of the fluid dissipating into the air or missing the catch tray. After cutting the final optical surfaces, the optic was measured on the Zygo Nexview. The surface was dominated by mid spatial frequency errors ranging in wavelength from 100 to 175 μm. The surface measurement was filtered to the waviness regime of 80 μm to 2.5 mm, Figure 4.4.

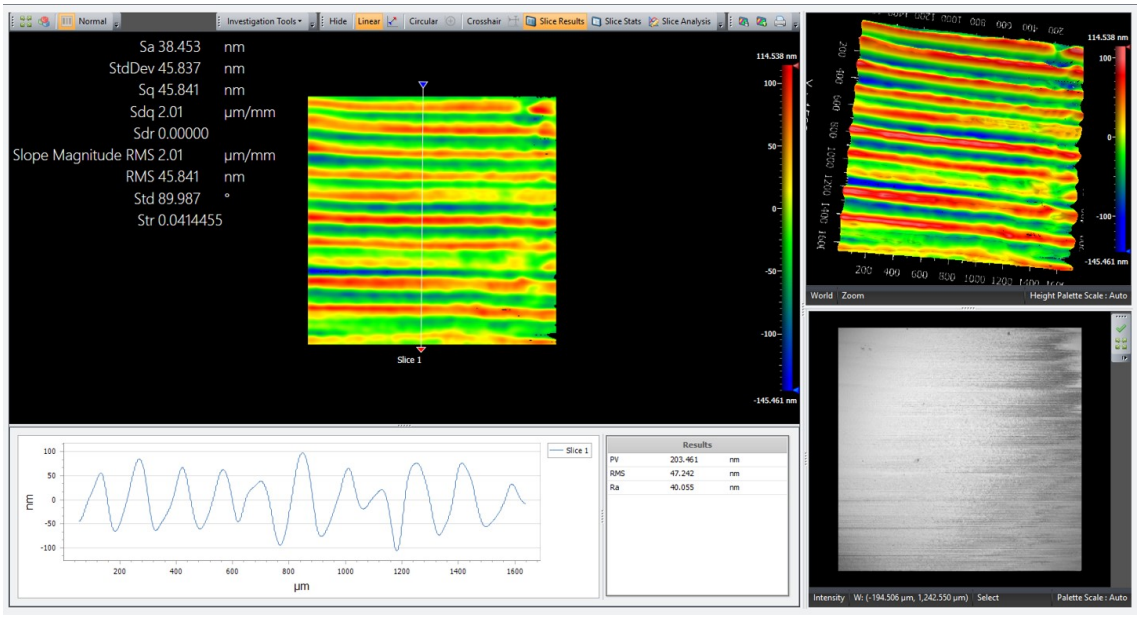

Figure 4.4: Mid-spatial in the finish optical surfaces of iteration one.

The wavelength of the mid-spatial corresponded directly to the timing of the coolant re-circulation pump. The pump would warm the fluid every 8.8 minutes. The warm fluid would warm the part and cause the polycarbonate to expand. The fluid would cool and the part would shrink again. The machine was cutting at 100 mm/min for 35 mm at a step over of 10 μm in a single direction raster. After a single raster, the machine would move 35 mm at 200 mm/min to the start of the next raster. This results in about 0.525 min/raster and 17 passes per cycle of the pump. At the 10 μm step over this results is 0.17 mm of rastering per cycling of the pump. which agrees with what was found in the

4.2 Cutting Fluid Type

Based on research and testing, WD-40 was used for the cutting fluid. WD-40 is a liquid coolant with solids in suspension. The solids would clog the delivery nozzle so they were filtered out of the fluid to prevent clogging. Once the optical surfaces were created, they were left with WD-40 residue which was not removed with an isopropyl alcohol drag wipe and spray. The optic had to soak in dawn soap and warm water in an ultrasonic cleaning system to remove about half of the residue. Another quarter of the residue was removed with dawn soap soak and drag wipe. This was a tedious process that risked damaging the optical surface. Due to the residue, Odorless mineral spirits were used for the multi-surfaced free-form demonstrator in iteration two.

4.3 Iteration 2-Multi-sided Free-form Manufacturing

Iteration two multi-sided free-form prism is the manufacturing of the proposed prism in Section 4.3.1. This iteration builds on iteration one and implements changes based on iteration one lessons learned.

4.3.1 Optical Demonstrator Design

The demonstrator for this project must have multiple freeform surfaces and the system must be designed such that re-fixturing during the manufacturing process is required to complete the system. The selection of the demonstrator was determined by recommendations from CeFO members; a list of multi-surfaced systems was created for consideration. A multi-sided three surface optical prism was selected by popular vote and was designed to fit the requirements for this project. Polycarbonate was selected for the material because of its light weight and it was of the most interest by the CeFO members.

The selected design, Figure 4.5 is compact and has an intended use for head worn displays, virtual reality, or augmented reality.

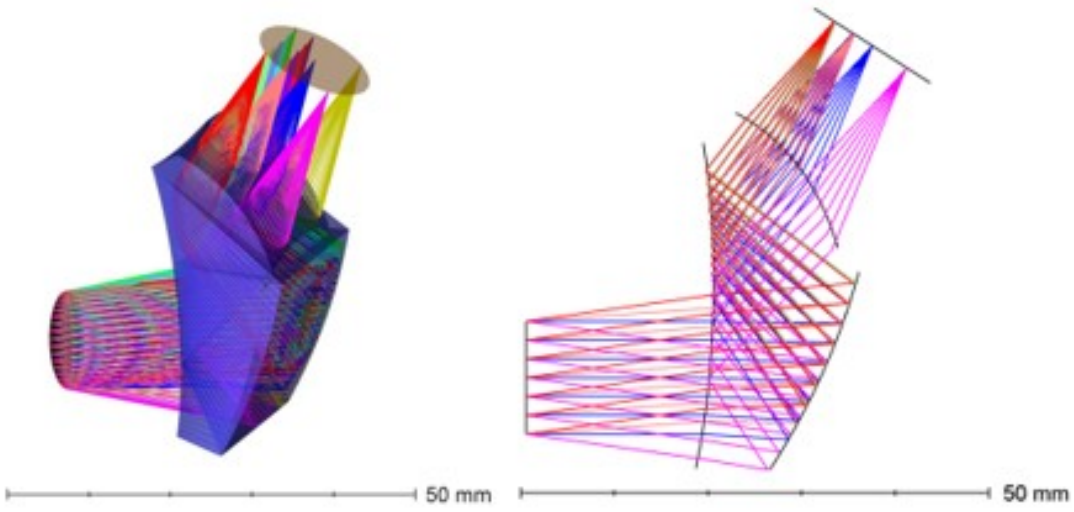

Figure 4.5: Multi-surface freeform demonstrator.

Figure 4.6 illustrates the functionality of the multi sided prism. Light comes in from the object plane, reflects off of surface one through total internal reflection on to surface two. Light then reflects off of surface two, also with total internal reflection and transmits through surface one to the eye box. A reflective coating can be installed on surface two to increase performance. The intent of this system is to have a persons eye at the eye box and an illuminated display with spatial contrast at the object plane. This creates an overlay of the image shown at the object plane onto the image seen to the right of the system.

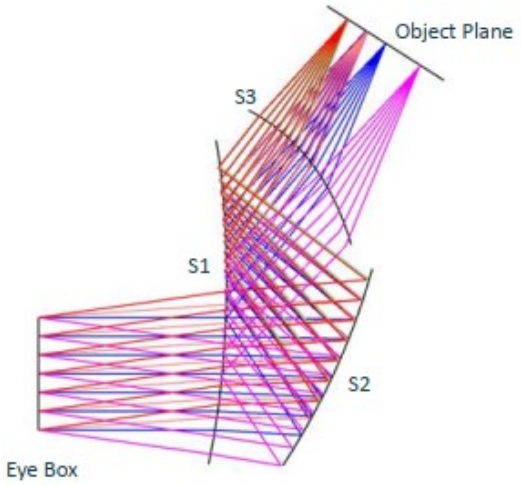

Figure 4.6: Multi-surface freeform demonstrator operation

Quantitatively testing an optical system after manufacturing is complicated. The easiest first test is to compare a simulated image with a captured image from the final system. Figure 4.7 shows the distortion of a city landscape image due to the optical design. Comparing this and the same image though the final optical assembly will provide a good estimate as to if the qualitative behavior is as designed.

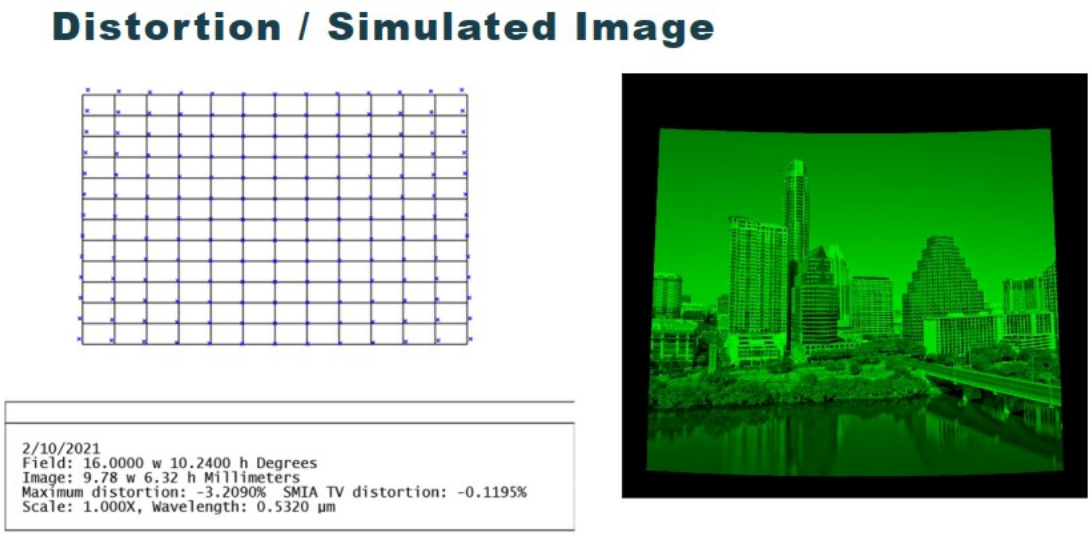

Figure 4.7: Multi-surface freeform demonstrator simulated image.

4.3.2 Fixturing

The fixturing of the multi sided optic has two main aspects: (a) surface registration and reach and access (b) mechanical holding force by vacuum. First the optical prism needs to be mounted in a fixture that allows all surfaces to be manufactured while simultaneously allowing referencing of each surface relative to the others. Essentially reach and access and surface registration must be attainable. Second is the vacuum fixturing that mounts the prism and frame to the diamond turning machine. The fixturing for the optical prism was based on the fixturing from iteration 1 but resolved the issues with the monolithic polycarbonate design. This fixturing system must be stiff enough to not deform when clamped in the vise. The design must also be able to incorporate datums for manufacturing and metrology references. Figure 4.8 shows the final design with incorporated datums.

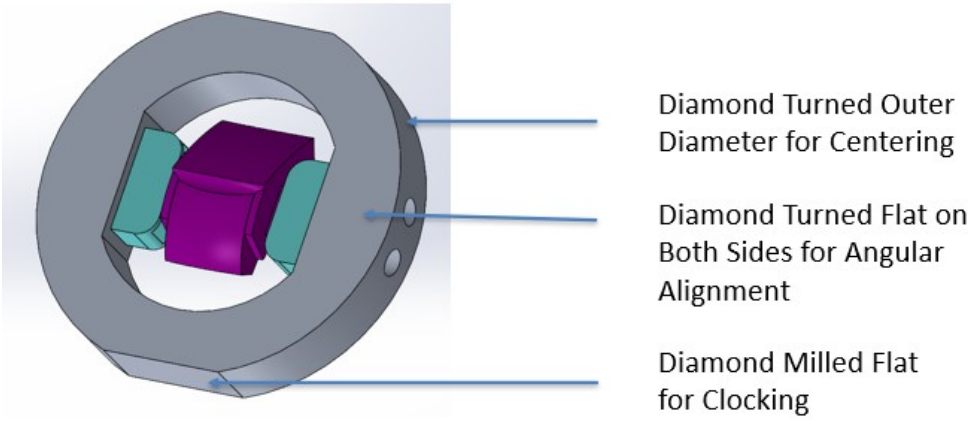

Figure 4.8: Optical prism fixturing design.

This design is made of 6061-T6 aluminum which is significantly stiffer than polycarbonate. There are three alignment datums which were created in the manufacturing of the front side of the multi-sided free-form prism. The first is the diamond milled flat which aligns the clocking of the optic. Diamond turned faces allow for angular and piston alignment and a diamond turned outer diameter centers the optic. All degrees of freedom are referenced which allows for alignment from manufacturing to

metrology.

Figure 4.9 illustrates how the multi-sided prism is mounted and oriented in the fixture.

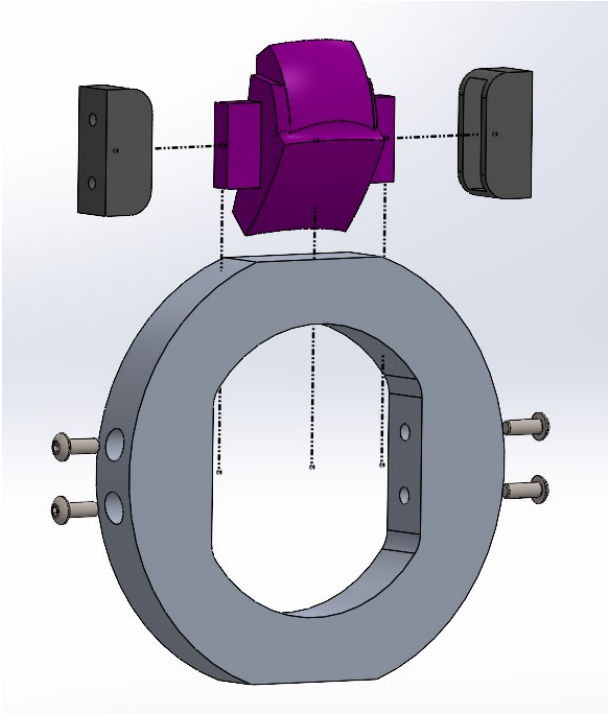

Figure 4.9: Exploded optical prism fixturing design.

To start, a polycarbonate rectangular prism was manufactured on the Haas CNC mill. On two sides of the prism, a tab was manufactured and is shown in Figure 4.10.

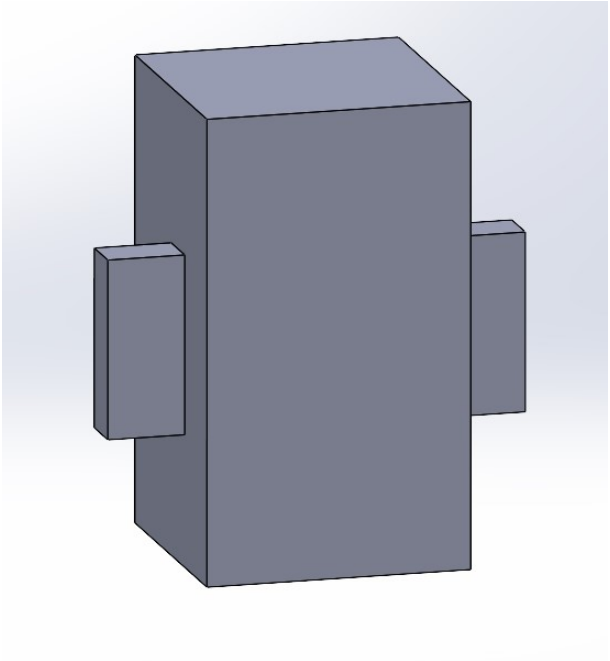

Figure 4.10: Optical prism roughing blank.

Epoxy was then mixed up and poured into the fixturing ring tabs. Each tab was placed onto a corresponding tab on the polycarbonate prism, as shown in Figure 4.11.

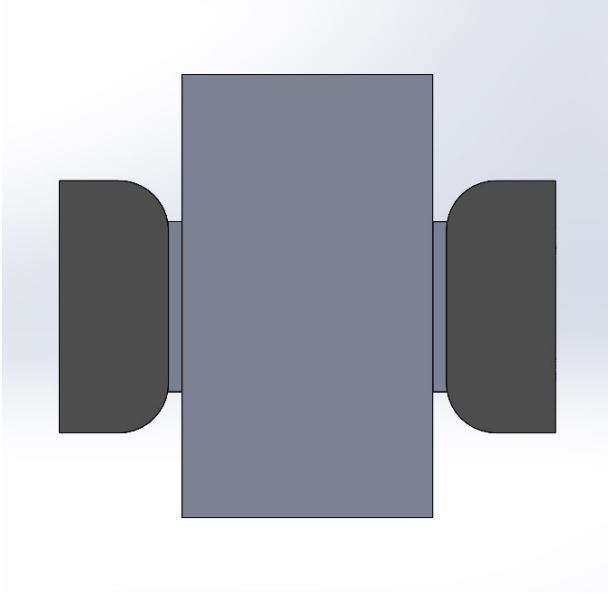

Figure 4.11: Optical prism mounted into fixturing tabs.

Before the epoxy is fully cured, the fixturing tabs and polycarbonate prism are located inside the fixture and screwed down using the four screws shown in Figure

4.9. Installing the fixturing tabs and polycarbonate prism into the fixturing ring helps to reduce deformation errors while fixturing the optic. During the manufacturing process we would ideally hold the optic without deforming it such that when the optic is released it doesn't relax to a different shape. Hard fixturing the fixturing tabs while the epoxy is considerably more pliable than the polycarbonate prism reduces relaxation distortion when the optic is removed from the fixturing ring. The system, Figure 4.12, was left to fully cure before the near net prism is manufactured.

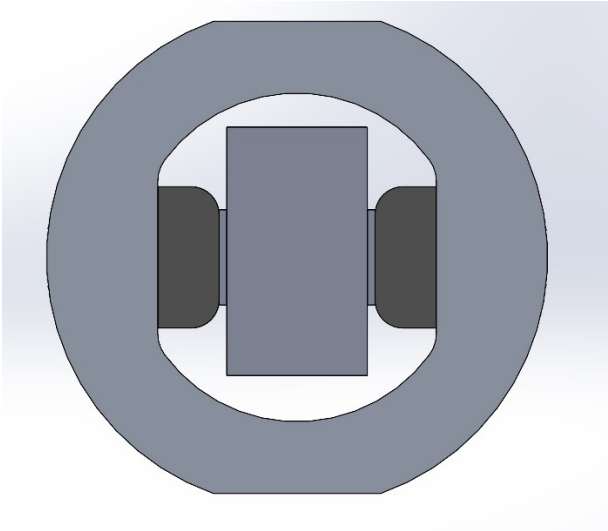

Figure 4.12: Optical prism mounted into fixturing assembly.

The cured assembly was then taken to the Haas office mill where it was installed in the vise with the minimum amount of force required to hold the system in place without moving. Tightening the system too tight in the vise can cause the fixturing ring to elastically deform so much that the near net optical surfaces become over cut. The required tools for the office mill were then set up and the MasterCAM generated near net milling programs were ran. This was repeated on the other side of the system. Nominally, 254 microns of material was left on the optical surfaces for the near net shape. This allows for there to be material left when the ultra precision milling operations are ran on the diamond turning machine.

Once the fixturing was designed and the near net optic was machined, the vacuum

chuck, Figure 4.13 that holds the fixturing assembly and the optic to the diamond turning machine was designed and manufactured.

Figure 4.13: Custom vacuum chuck.

The chuck incorporates multiple vacuum channels that are adjustable so that smaller diameter systems like the centering pin can be mounted to it. The center of the chuck has a cavity so that prisms that protrude from the fixturing ring can be mounted to it without coming in contact with the vacuum chuck.

4.3.3 Surface Generation and Validation

A critical part of this entire process is the generation and validation of the optical surfaces.

4.3.3.1 Optical Designs and Prescriptions

When a design is sent from the optical designer for manufacturing, four items are included. The first is a three-dimensional model of the system and the second is a drawing of the system with dimensions that locate the optical surface centers in space. The third item provided is the formula and prescription of the optical surfaces. The

final item in the design package is a set of tables that describe the sag of the optical surfaces. A true design package should also include tolerances for the surface locations and shape. This design did not include tolerances. It was to be manufactured to the best of our abilities.

The 3D model of the system is shown in Figure 4.14. In the case of the system used in this project it was in the form of an STL (stereolithography file type).

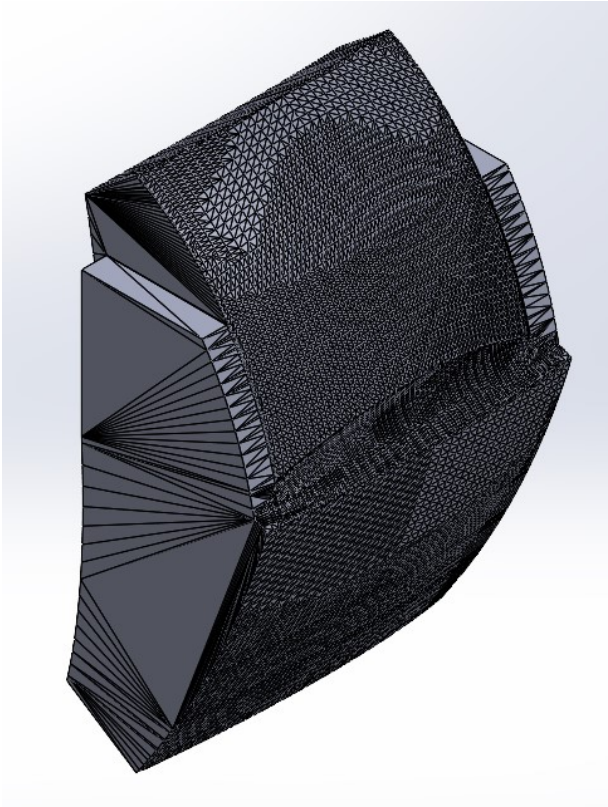

Figure 4.14: Provided STL model.

The drawing of the optical system with surface references is shown in Figure 4.15. One of the drawings specifies the linear translations of the surface centers from the defined datums and the other specifies the angular orientation of the surface center normals relative to the drawing datums.

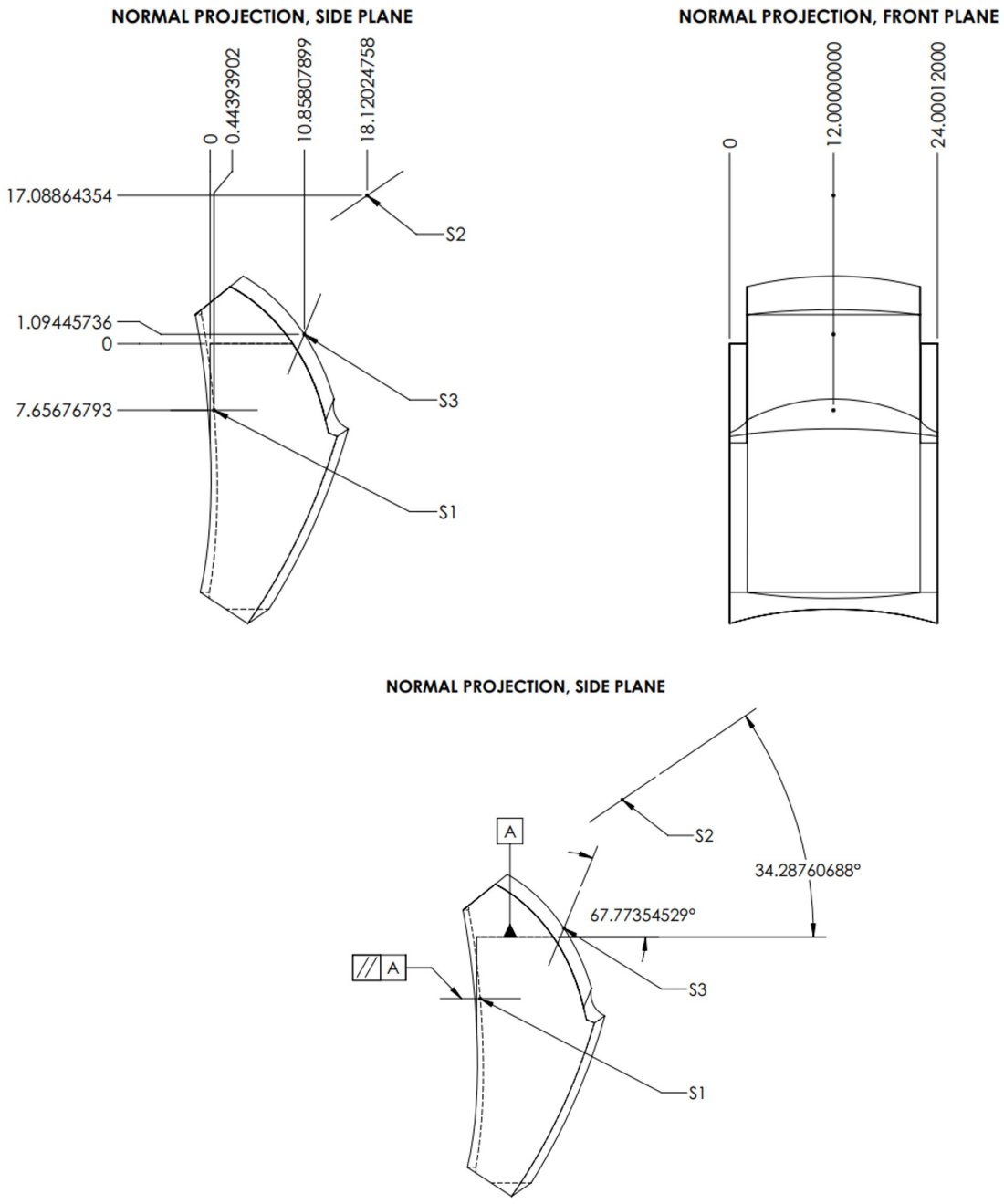

Figure 4.15: Provided drawings.

The location of the image and object plane are also defined in a supplied drawing, Figure 4.16.

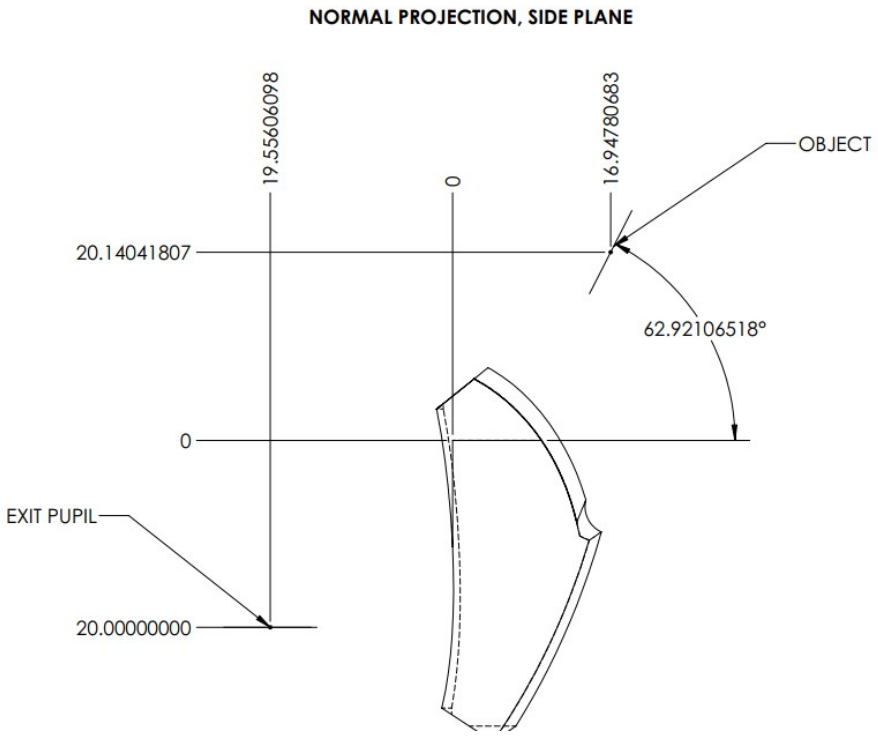

Figure 4.16: Provided object and image plane drawings.

These drawings were used to place the surface centers, object plane, image plane, and ray trace onto the optic to ensure that there was room for testing during the design of the fixturing system. This is shown in Figure 4.17.

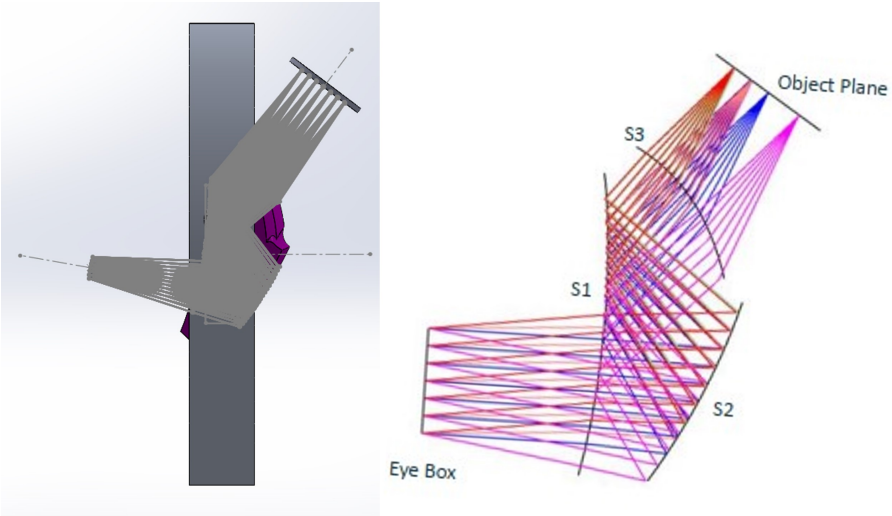

Figure 4.17: Raytrace, object plane, and image plane overlaid onto the 3D model.

The optical designer created the demonstrator using an extended polynomial prescription formula, Eq 4.1.

$$Z = \frac{cr^2}{1 + sqrt(1 - (1 + k)c^2r^2)} + \sum_{i=1}^{N} A_i E_i(x, y) \tag{4.1}$$

Where Z is the resulting sag,

k is the conic constant,

c is the curvature,

r is the radial coordinate,

N is the number of the polynomial coefficient in the series,

A_i is the coefficient on the ith polynomial term, and

E_i is the polynomial term associated with the ith polynomial term.

The final item in the design package from the optical designer was a set of tables that describe the sag or surface center normal height distribution over a finite number of grid points on the surface. These are used as a refernce to verify that the prescription that was written down matches the theoretical output of the optical design software.

4.3.3.2 Surface Comparison

Once the manufacture receives the optical design package, it is there job to make sure that the prescription matches the provided reference sag tables. This is completed to ensure there is no typos or errors that could result in the manufacturing of the wrong surfaces. The prescription and sag table are loaded into MATLAB. The surfaces are generated based on prescriptions and the provided tables are compared to them. If the error between the provided sag table and the generated surface is significantly small, then the two agree with each other. Figure 4.18 shows the error between the three generated iteration two surfaces and their corresponding sag tables.

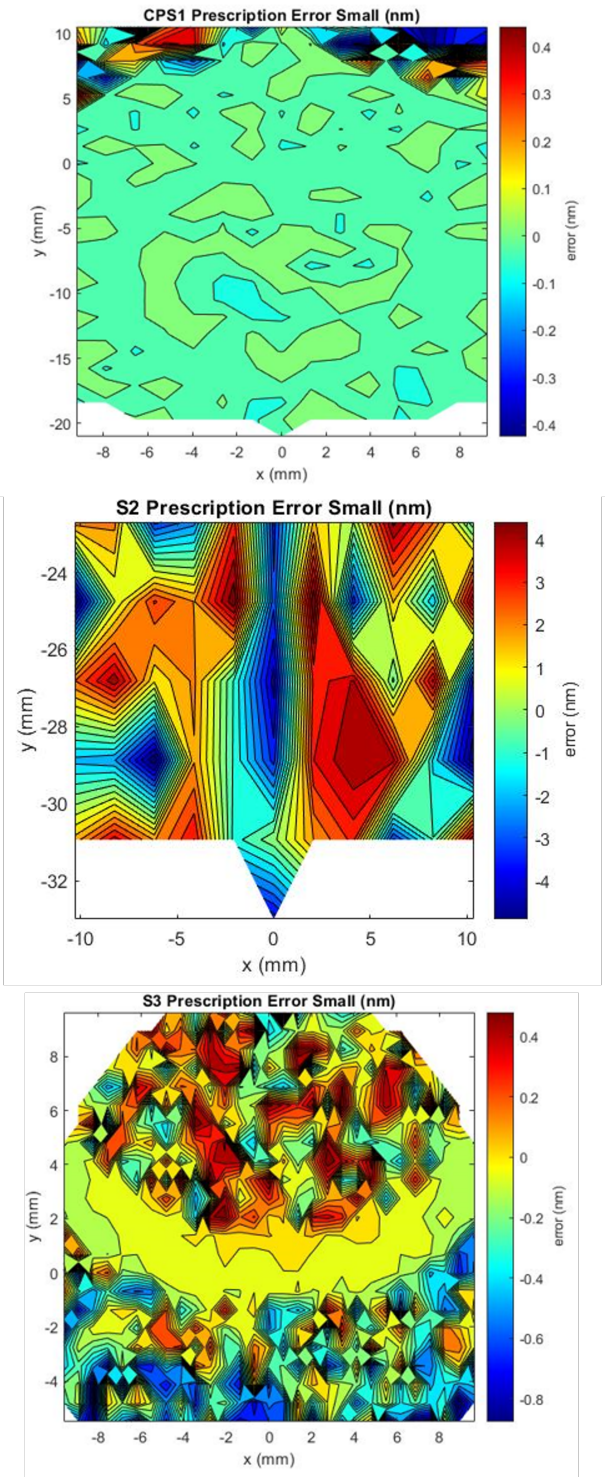

Figure 4.18: Error maps of the generated prescription and the provided sag tables.

4.3.3.3 NanoCAM Surface Import and Comparison

NanoCAM, the tool path generation software currently does not accept extended polynomial surfaces as an input. High density point clouds of the surfaces were generated and exported to text files using MATLAB. These were then imported into NanoCAM and NURBs based surfaces were created from them. The three dimensional model with fixturing was also uploaded into NanoCAM. Using the provided drawing and the three dimensional model, the surfaces were rotated and shifted into place. NanoCAM has a feature that can then compare the three dimensional model surfaces to the generated surfaces. If the error between them is significantly small then all four items in the design package agree.

4.3.4 Tool Path Generation

Now that all the surfaces are loaded into NanoCAM, the tool path generation can begin. The roughing passes were generated first, then the final finish passes were generated using the steps outlined below. Roughing passes were cut at a 40 μm step over, 150 mm/min feed rate, and 50 DOC. The finish passes were cut at a 10 μm step over, 100 mm/min feed rate, and 10 DOC.

1. Set up the milling tool and find the tool geometry values

   (a) The milling spindle was balanced to 5 nm of imbalance at a spindle speed of 40,000 RPM

   (b) The tool was corrected to a PV error less than 200 nm and is shown in Figure 4.19 and 4.20. The milled sphere radius was reported to be off by only 32 nm and and the diamond offset was reported to be off by 120 nm. At this point any corrections to the tool would not improve the PV error.

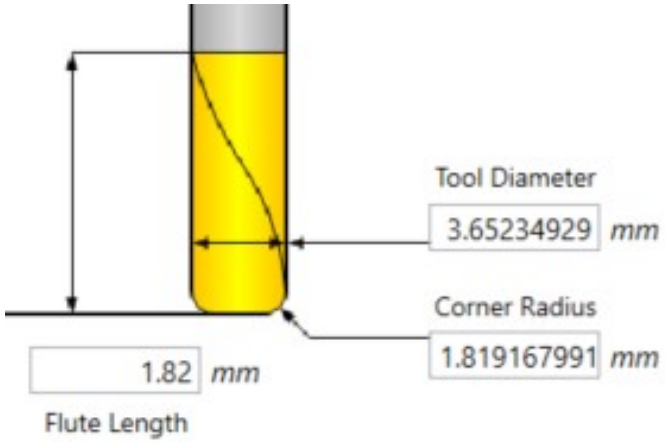

Figure 4.19: Corrected tool geometry.

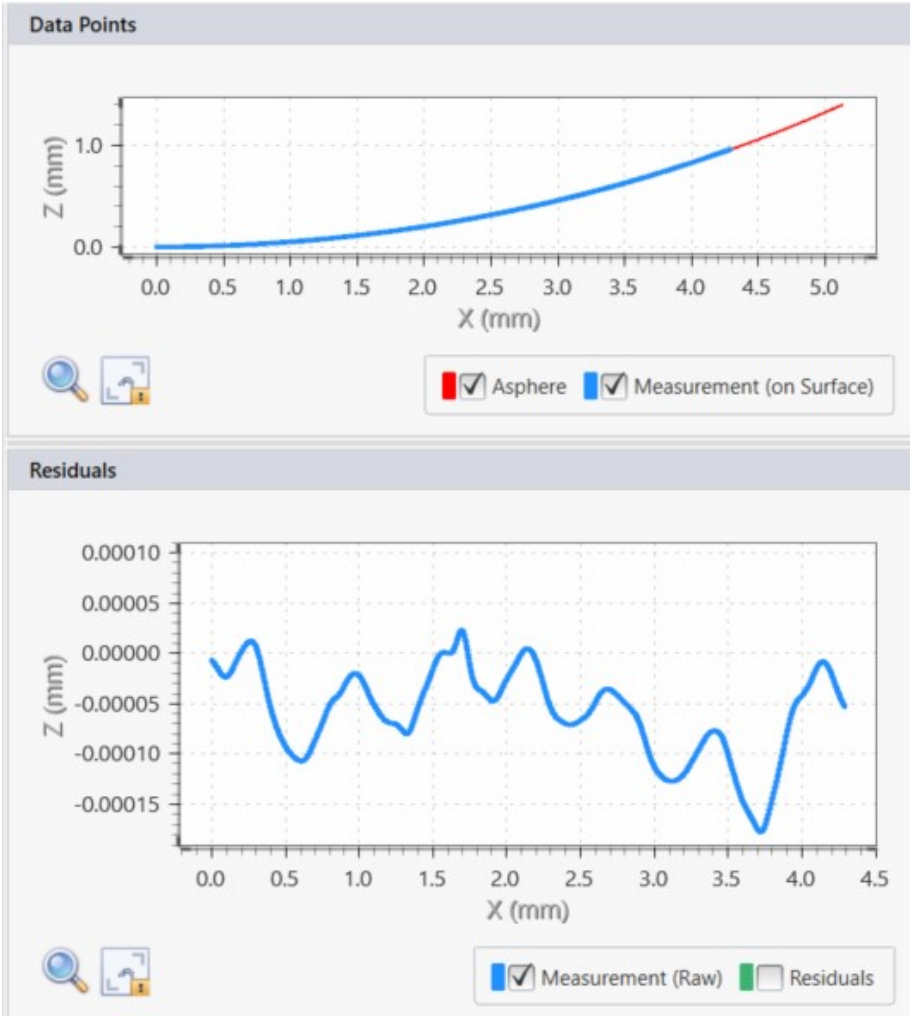

Figure 4.20: Remaining tool correction error

2. Define the milling tool in NanoCAM with the tool number that matches the tool number offsets in the machining center
3. Define an operation that fits the surface. Iteration 2 was completed with X, Y, Z three axis milling.
4. Select the surfaces to cut
5. Define the feed parameters: Direction, feed rate, and step over
6. Define linking and path entry parameters
7. Select surfaces to avoid
8. Generate the tool path
9. Look over and simulate the tool path to ensure proper motion and no visible errors or collisions
10. Post process the code for that operation

4.3.5 Cutting Fluid Delivery

Iteration one cutting fluid delivery was far from perfect. It introduced mid-spatials that greatly effected the quality of the image. The system had to be redesigned to remove items that could produce thermal effects on the optic. A venturi vacuum pump for traditional machining applications was used to transport the fluid from the catch container to the pressure container instead of the pump, Figure 4.21. The new pump required an air line so the pressure line was removed from the tank and used for the pump. The pump then pressurized the container while transferring fluid to it.

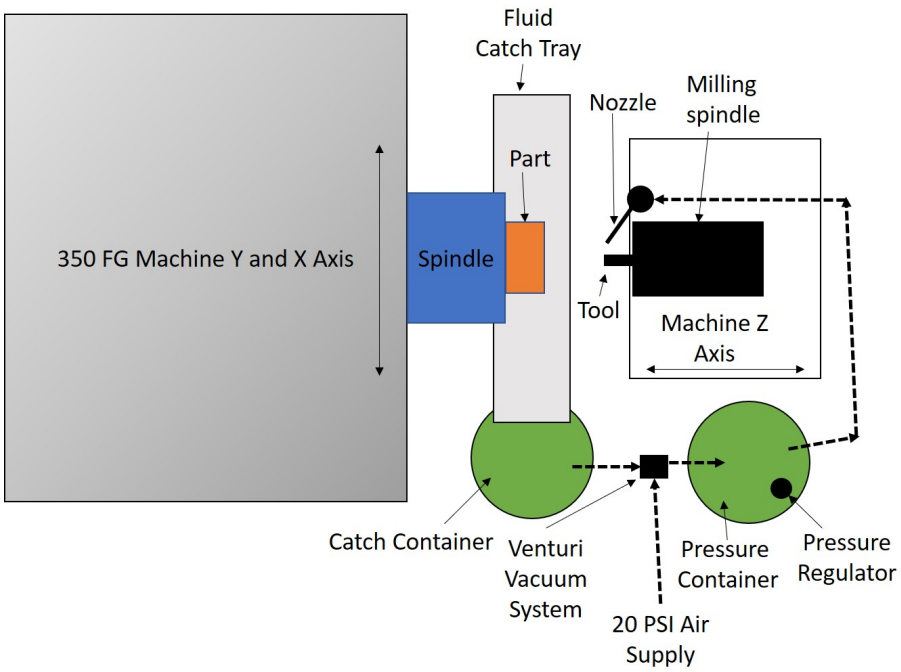

Figure 4.21: Milling coolant system with venturi pump.

The pressure regulator is to adjust the pressure in the pressure container to ensure the proper flow to the nozzle. It must also be set to ensure that the pump is filling the pressure container at a rate that is higher than the container is emptying.

4.3.6 Manufacturing Procedure

The manufacturing of multi-sided optics is not as simple as mounting an optic roughing and cutting it. To help ensure that surfaces on opposite sides of an optic have the correct dimensional relationship to each other a specific procedure was developed and tested. The following describes the manufacturing process of a desired multi-sided optic. In this manufacturing scenario, the desired optic is shown in Figure 4.22.

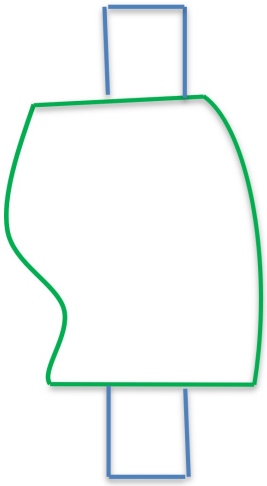

Figure 4.22: Milling and coolant.

The process includes a series of steps that start with the manufacturing of a vacuum chuck that can receive and hold the optical assembly. The roughing of the optical assembly is then created on a non precision or precision machine like a Haas toolroom mill, Figure 4.23.

Figure 4.23: Roughing of the optical assembly using the haas tool room mill.

Leaving 5 to 10 thousandth of an inch on each surface is sufficient but more might

be needed based on the tolerances of the machine that is used to rough in the optical assembly. This procedure helps to ensure that there will be enough material left on the other side when the optic if flipped. Figure 4.24 shows the optical assembly mounted in its vacuum chuck. The green outline is the desired optic and the blue outline is the roughed in optic.

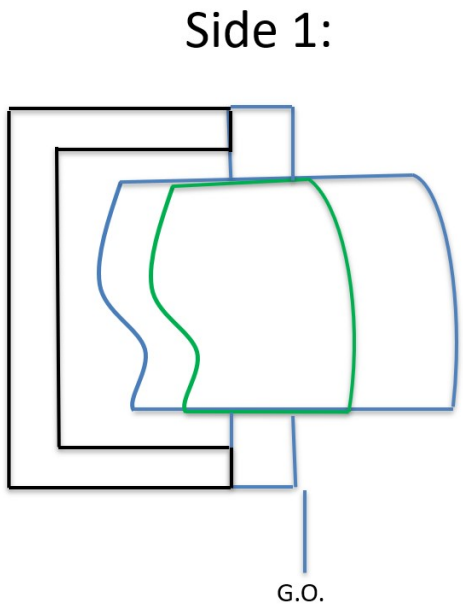

Figure 4.24: Starting (blue) and desired optic (green).

Once the part is centered, aligned, and the tool is set up, the optical roughing can begin. The system mounted on the 350 FG diamond turning machine is shown in Figure 4.25.

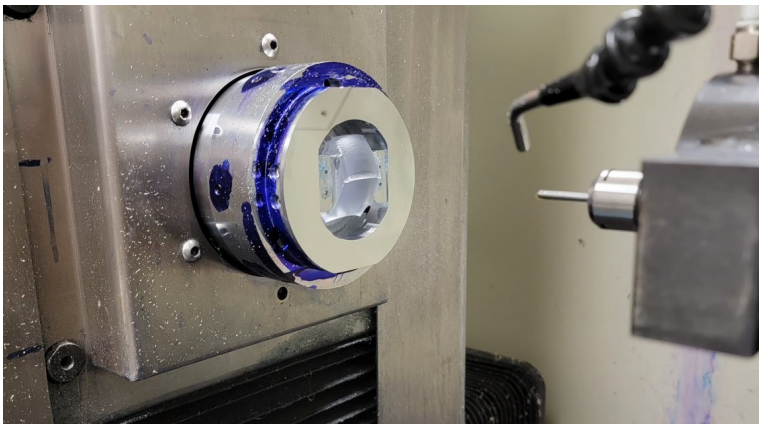

Figure 4.25: Roughed optical assembly set up on the diamond turning machine.

Figure 4.26 illustrates the following. The fixturing ring surface is diamond turned and a global origin, G.O. is defined at that surface. The milling tool was used to ultra precision machine the outer diameter of the aluminum reference ring for a centering reference. A flat was also ultra precision milled for clocking alignment reference. The work coordinate system (WCS) of the machine is offset away from the G.O. by at least the amount left on the surface by the non precision roughing procedure. A roughing pass is made on the ultra precision machine. If the surface was not completely cut then the work coordinate system is offset into the part and another roughing pass is made. This is repeated until the entire surface has been cut. Once roughing is completed, the WCS is offset inward one last time for a finish pass. The amount of offsets, roughing and finish, is added up and subtracted from the initial WCS offset. This value is defined as Z.

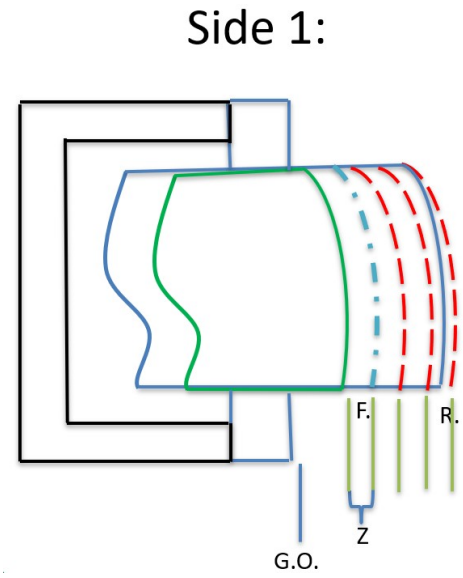

Figure 4.26: Side one manufacturing steps illustrated.

The optical assembly is then carefully removed from the vacuum chuck. The optic is then flipped over, mounted to the vacuum chuck, centered, and aligned. Once flipped, the G.O. is found by touching the tool off of the face of the vacuum chuck. A new WCS is offset from the G.O. WCS inward (negative z direction) by Z amount. This offset accounts for the amount of material that was not cut on the first side of the optic and helps to ensure that the second side has material left to cut. Figure 4.27 shows the optical assembly flipped on the vacuum chuck. The WCS is then offset out of the part by the finish cut depth of cut. A series of roughing passes on the ultra precision machine are ran to remove excess material.

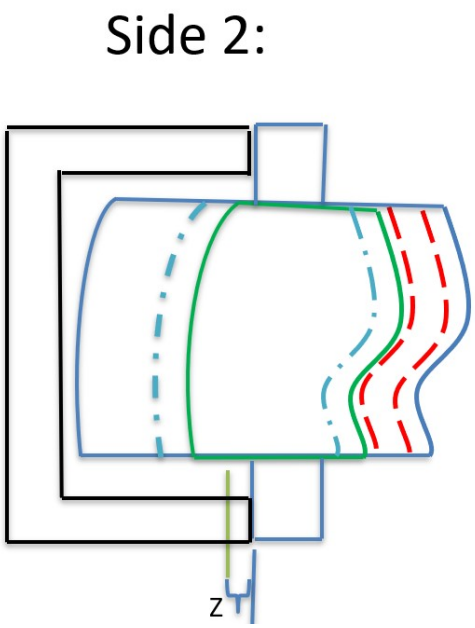

Figure 4.27: Side two manufacturing steps illustrated.

The WCS is then offset in by the finish cut DOC and a finish pass is ran, resulting in Figure 4.28

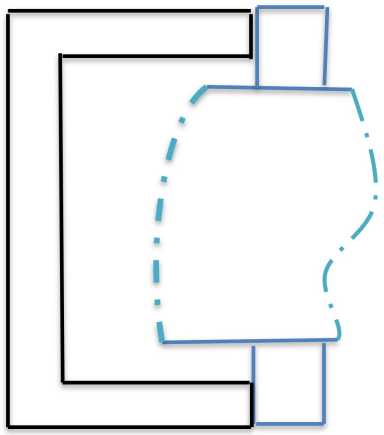

Figure 4.28: Final optic.

CHAPTER 5: Basic Metrology and Functional Testing

5.1 Completed System and Visual Inspection

The optical surfaces were very clear with no visible haziness like what was seen in the iteration one optical surfaces. Figure 5.1 shows the final optic in the fixture.

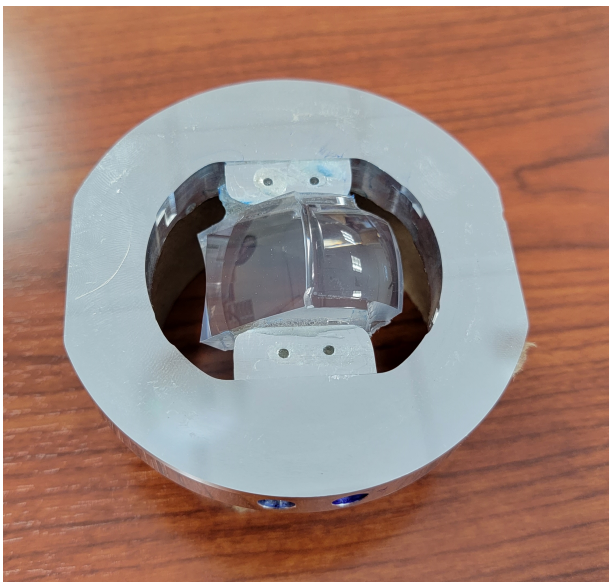

Figure 5.1: Final optic in the fixture.

5.2 Surface Roughness

The measurements were taken on the Zygo Zegage Plus with a 20x and 50x objective. Each measurement was completed with averaging set to two. Post processing involved the removal of 4th order form and the application of a roughness filter. The roughness filter was defined as features on the surface with a wavelength greater than 2.5 μm but less than 80 μm in accordance with ISO-10110-8:2010 section 4.3. A three sigma spike clip and an edge clip was performed as part of the post processing. Figure 5.2 shows the roughness measurement of surface 1 and 2 with the 20x and 50x

objective. (see 4.6 for surface references).

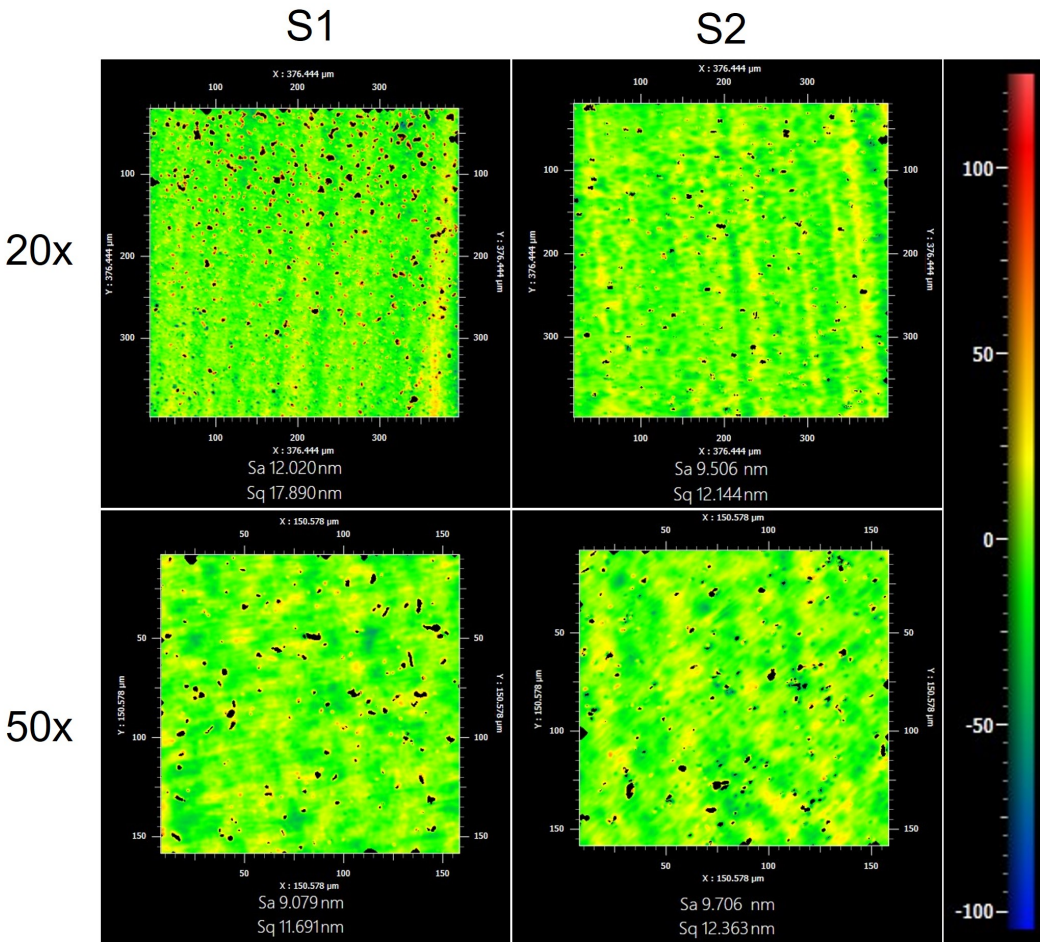

Figure 5.2: Surface roughness of S1 and S2.

It can be seen that there is some residue or re-adhered chips remaining on the optical surfaces. The cleaning procedure was spraying the optical surfaces with isopropyl alcohol and clean air. Additional cleaning of the optical surfaces can be completed and will likely remove the residue or chips. There is always a risk of damaging the surfaces more when they are cleaned which is why no additional cleaning of the surfaces was completed. The surface roughness of the optical surfaces was agreed with the roughness found during the patch testing in Chapter 3.

5.3 Qualitative Functional Testing

Initial qualitative functional testing of the iteration two optic was completed by placing an illuminated display at the object plane and a detector at the eye box. Figure 5.3 shows the optical system with the placement of two cellphones to functionally test the optical system.

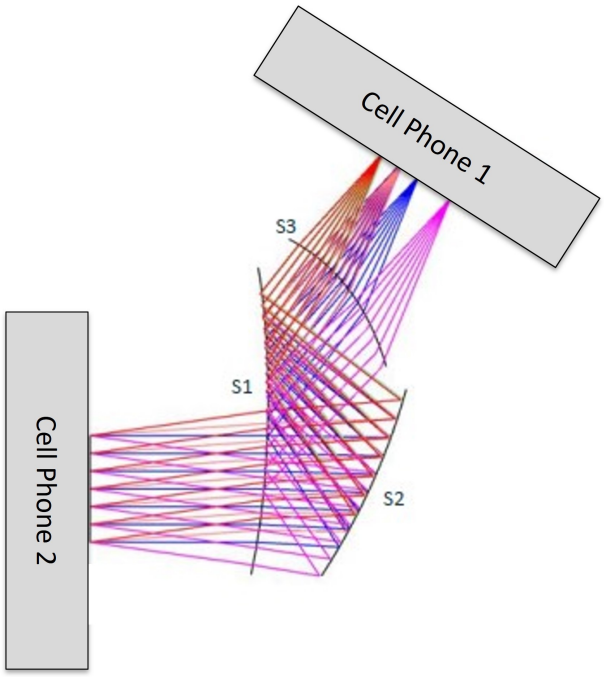

Figure 5.3: Functional testing setup.

An Air Force test chart, Figure 5.4 was illuminated on cell phone 1 screen.

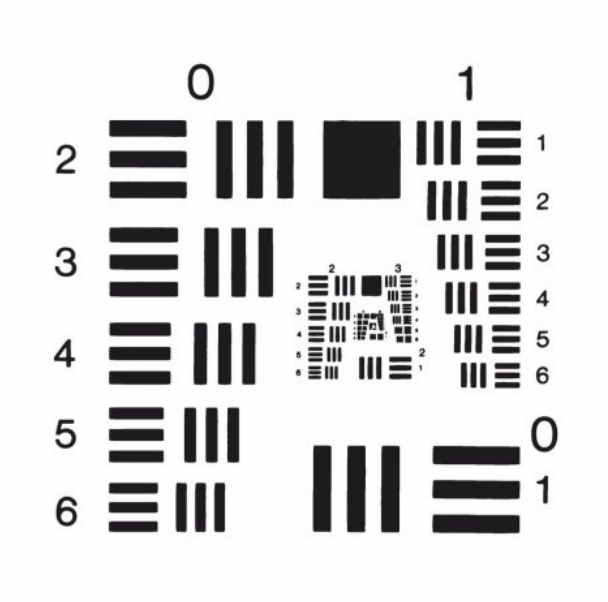

Figure 5.4: Air force test chart.

The camera of cell phone two was placed at the eye box as best as possible. Figure 5.5 shows the image of the Air Force test chart overlaid on a solid back drop.

Figure 5.5: Air force test chart imaged by cell phone 2.

When imaged on a non solid back drop with more light, Figure 5.6, the overlaid image did not appear as clear or bright when compared to the solid background.

Figure 5.6: Air force test chart imaged by cell phone 2 without a solid background.

There was some distortion in the overlaid image which was likely from the placement of the cell phones not being exactly at the eye box and object plane.

5.3.1 Planned Functional Testing

Additional advanced functional testing will be completed in the near future. This testing will involve the knife-edge test which is a standard method of characterising image quality. For the iteration two system, a razor blade will be fixed to the front left of the system shown in Figure 5.7, at the object plane.

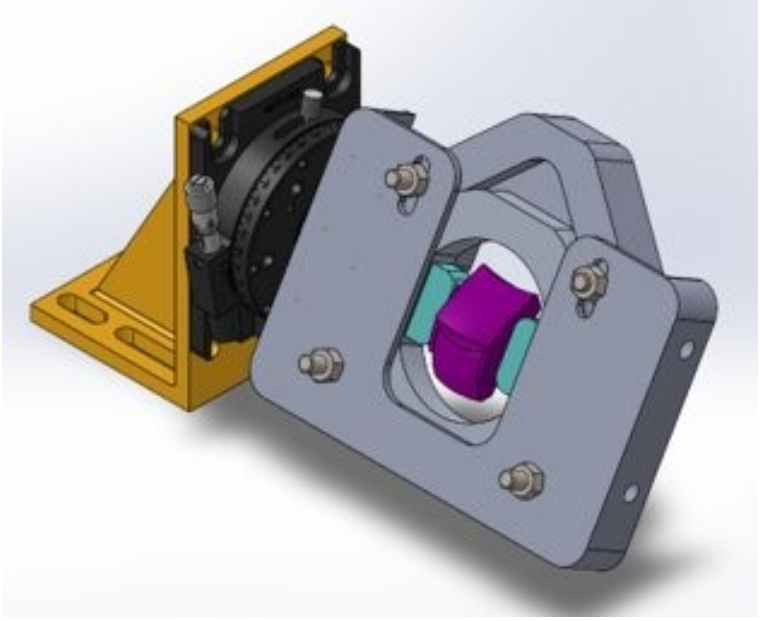

Figure 5.7: Preliminary knifes edge testing set up.

The razor will be back illuminated. A focusing lens and detector will be placed at the image plane. The detector will image the back lit razor blade and determine if the system is detector or optically limited. A detector limited system will have a resulting image that has full zero to unity contrast within a single pixel. A system that does not have this is optically limited and a modulation transfer function (MTF) can be backed out of the image. Different MTF profiles can be determined based on the orientation of the razor edge [41, 42].

CHAPTER 6: Future Work

Future work is needed to verify the form accuracy of the optics. Current metrology methods are not capable of easily measuring systems with such large sag and steep slopes. The manufacturing methodology described in this document was designed to address the gap in manufacturing methods related to these systems but there is also a gap in the metrology methods required to measure such systems. Manufacturing and metrology references were developed and manufactured into the optical system but a true metrology methodology is required to fully develop the required system datums for accurate measurements of the surfaces and there relationship to one another. Functional and optical testing of the iteration two system will be performed to evaluate the optical performance of the system. This will give an idea as to how well the optic was manufactured.

The methodology in this thesis is designed for prototyping and one off optical systems. Like most ultra-precision manufacturing processes, the set up and cycle times are long and tedious. Mass manufacturing these systems using this process is impractical and expensive. Injection molding, or equivalent processing, of these system is something that needs to be further researched in order to reach a mass production cost and time model.

Geometric tolerancing of the surfaces is something that also requires further exploration. The optics manufactured during this thesis, and many others are designed and manufactured without surface tolerance specifications. Further work needs to be completed to define tolerances for the surface locations relative to each other and the shape of the surfaces. This project was to complete the system to the best of our abilities with no tolerance specifications in mind.

CHAPTER 7: Conclusion

The ultra precision manufacturing methodology of a complex multi-sided, multi-surface optical prism has been demonstrated through the manufacturing of a polycarbonate prototype system. The prototype material, polycarbonate was an unfamiliar material to the University of North Carolina at Charlotte freeform optics group. Through thorough research and testing, optical quality surfaces where achieved. The literature research provided a solid foundation of cutting parameters to start our patch testing with. Patch testing with varied depth of cut, feed rate, step over, and lubricant/coolant type defined a set of parameters that provided optical quality surfaces. A final set of parameters, Table 7.1 was chosen to balance surface quality and cycle time.

Table 7.1: Optical Surface Cutting Parameters

Parameter	Value
Tool Radius:	1.82 mm nominal
Rake Angle:	0 deg
Spindle Speed:	40,000 RPM
Feedrate:	100 mm/min
Stepover:	10 μm
Depth of Cut:	10 μm
Direction:	Climb Milling

The development of the iteration one optical system defined a starting point for the manufacturing of systems with multiple surfaces on multiple sides. Iteration two

implemented changes based on results from iteration one. Coolant type is important for the surface quality. The coolant must aid in reducing roughness by its properties but must also be easy to remove from the surface and not leave residue. WD-40 was able to produce better surfaces but at the cost of extensive cleaning when compared to odourless mineral spirits which was also capable of optical quality surfaces. The delivery of the coolant was also critical. The long cycle times required that the coolant be recycled. It is imperative that the re-circulation system not induce any heat to the coolant. Iteration one surfaces consisted of a considerable amount of waviness that resulted from the cycling of a re-circulation pump. This was fixed and the waviness was eliminated in iteration two. Implementation of lessons learned from iteration one resulted in the iteration two optical system to be far soupier from a roughness, visual inspection, and function testing point of view. The manufacturing of multi-sided freeform prisms has been completed in the past, but through rigorous development and testing there is now a documented manufacturing methodology to help others in the manufacturing of similar optical systems.

REFERENCES

[1] "Haas om series." Data Sheet PDF.

[2] "Zegage plus 3d optical surface profiler with sub-nanometer precision for non-contact surface measurement." Last retrieved 2022-04-07 from https://www.azom.com/equipment-details.aspx?EquipID=4395.

[3] G. P. Gubbels, "Diamond turning of glassy polymers," January 2006. Last retrieved 2022-03-20.

[4] M. S. Alan Symmons, "Field guide to molded optics," 2016. Last retrieved 2022-03-04.

[5] "Difference between conventional milling and climb milling." Last retrieved 2022-04-07 from https://www.mecholic.com/2018/05/comparison-upmilling-downmilling.html.

[6] "Choose the right tool." Last retrieved 2022-04-07 from https://robbjack.com/support-article/choosing-the-right-cutting-tool-for-the-mold-making-industry/.

[7] S. sai charan Bodlapati, "Diamond turning of plastic optics," 2019. Last retrieved 2022-03-20.

[8] W. H. Q. D. Julong YUAN, Binghai LYU, "Review on the progress of ultra-precision machining technologies," March 2017. Last retrieved 2022-04-05.

[9] L. C. L. F Z Fang, XD Liu, "Micro-machining of optical glasses â a review of diamond-cutting glasses," October 2003. Last retrieved 2022-03-16.

[10] R. W. C. Alan M Frank, James B Bryan, "Quick fast off-axis parabolas," November 1977. Last retrieved 2022-03-16.

[11] P. M. Paul Chrzanowski, Arnie Heller, "Lawrence livermore national laboratory 1952-2017," 2017. Last retrieved 2022-03-16.

[12] D. L. P. Shore, P. Morantz, "Manufacturing and measurement of the miri spectrometer optics for the james webb space telescope," 2006. Last retrieved 2022-04-05.

[13] A. M. Bauer, "Optical design with freeform surfaces, with applications in head-worn display design," 2016. Last retrieved 2022-03-16.

[14] J. P. R. Kevin P. Thompson, "Freeform optical surfaces: A revolution in imaging optical design," June 2012. Last retrieved 2022-03-16.

[15] W. T. Plummer, "Some milestones in the design, development, and manufacture of freeform optics," January 2019. Last retrieved 2022-04-05.

[16] L. Y. L. J. Y. G. Xiaodong Zhang, Fengzhou Fang, "Slow slide servo turning of compound eye lens," February 2013. Last retrieved 2022-03-19.

[17] R. J. Benjamin, "Diamond turning at a large optical manufacturer," November 1978. Last retrieved 2022-03-17.

[18] T. J. S. C. E. A. B. J. C. L. K. F. Jannick P. Rolland, Matthew A. Davies, "Freeform optics for imaging," February 2021. Last retrieved 2022-03-17.

[19] F. F. S. H. X. Z. Linlin Zhu, Zexiao Li, "Review on fast tool servo machining of optical freeform surfaces," 2018. Last retrieved 2022-04-05.

[20] Y. C. W.-Y. H. Chun-Chieh Chen, Chien-Yao Huang, "Ultra-precision diamond milling of aspheric microlens array," June 2013. Last retrieved 2022-04-05.

[21] E. U. Roland J. Benjamin, "Diamond turning of infrared optics," 1981. Last retrieved 2022-03-17.

[22] S. Kiontke, "Monolithic freeform element," September 2015. Last retrieved 2022-03-17.

[23] B. C. J. N. Todd Blalock, Brian Myer, "The manufacturing of a multi-surface monolithic telescope with freeform surfaces," 2019. Last retrieved 2022-03-17.

[24] M. A. D.-T. J. S. Michael L. Barkman, Brian S. Dutterer, "Free-form machining for micro-imaging systems," February 2008. Last retrieved 2022-03-17.

[25] "Visible light," 2010. Last retrieved 2022-03-19 from NASA Science website: http://science.nasa.gov/ems/09_visiblelight.

[26] "Application and environmental considerations for optical system design," September 2016. Last retrieved 2022-03-22 from https://escooptics.com/blogs/news/optical-materials-application-environment.

[27] "Optical material: Plastics." Last retrieved 2022-03-19 from https://www.emf-corp.com/optical-materials/optical-material-plastics/.

[28] "Optics materials: Glass versus polymers," February 2021. Last retrieved 2022-03-19 from https://www.addoptics.nl/optics-explained/optics-materials/.

[29] "Contact profilometers." Last retrieved 2022-04-07 from https://www.southampton.ac.uk/engineering/research/facilities /360/nCATS_facility/contact.page.

[30] "Why zemax?," 2022. Last retrieved 2022-03-19 from https://www.zemax.com/pages/why-zemax.

[31] "Math. graphics. programming.," 2022. Last retrieved 2022-03-22 from https://www.mathworks.com/products/matlab.html.

[32] "Design/engineering," 2022. Last retrieved 2022-03-22 from https://www.solidworks.com/domain/design-engineering.

[33] "Cad/cam software solutions," 2022. Last retrieved 2022-03-22 from https://www.mastercam.com/solutions/.

[34] "Optically precise nanocam4," 2022. Last retrieved 2022-03-22 from https://nanotechsys.com/nanocam/v.

[35] R. S. W. Blackley, "Ductile-regime machining model for diamond turning of brittle materials," April 1991. Last retrieved 2022-04-07.

[36] "List of thermal expansion coefficients (cte) for natural and engineered materials." https://www.msesupplies.com/pages/list-of-thermal-expansion-coefficients-cte-for-natural-and-engineered-materials Last retrieved 2022-03-19.

[37] A. S. Eric Marsh, "Measurement and simulation of regenerative chatter in diamond turning," 1998. Last retrieved 2022-04-09.

[38] S. W. Z. Z. S.J. Zhang, S. To, "A review of surface roughness generation in ultra-precision machining," February 2015. Last retrieved 2022-03-20.

[39] K. W. N. Schaal, F. Kuster, "Springback in metal cutting with high cutting speeds," 2015. Last retrieved 2022-04-09.

[40] "Optics and photonics â preparation of drawings for optical elements and systems â part 8: Surface texture," 2019. Last retrieved 2022-04-09.

[41] "Characterizing digital image acquisition devices," August 1990. Last retrieved 2022-04-18.

[42] "Modulation transfer function in optical and electro-optical systems," 2001. Last retrieved 2022-04-18.

APPENDIX A: Surface Comparison and Generation MATLAB Scripts

```
%Prism: S1
        clear
        clc
        clf
        close all
% Symbolic Variables
        syms poly rho X Y
% Parameters
        R_CAx=18; % Clear aperture radius mm
        R_CAy1=18;
        R_CAy2=18;
        R_CA=17.5346880000;


        Xneg=-9.18750000;
        Xpos=9.18750000;
        Yneg=-21.000000;
        Ypos=10.5000;



        R_norm=60; % Normalization Radius in mm
        k=-1.00003404920954; % Conic Constant
        R_curv=-5.38523977023703; % Radius of curvature in mm
        Cu=1/R_curv; % Curvature in 1/mm
            %sag table spacing


% Load the polynomial Coefficients
```

```
        load('powerCPS1.txt')
        K=powerCPS1;

% Load Sag Table
        load('CPS1_Sag_Table.txt')
        z_sag=CPS1_Sag_Table;

%Make the cartesian grid for the sag table imported
        [x_sag,y_sag]=meshgrid(-R_CA:2*R_CA/32:R_CA,R_CA:-(2*R_CA/32):-
           red↪ R_CA);

% Calculate Polar Coordinates Corresponding to Sag Table Points
        [phi_sn,rho_sn]=cart2pol(x_sag,y_sag);

% Load Sag Table small
        load('CPS1_Sag_Table_small.txt')
        z_sagsmall=CPS1_Sag_Table_small;

%Make the cartesian grid for the sag table imported
        [x_sagsmall,y_sagsmall]=meshgrid(Xneg:abs(Xneg-Xpos)/14:Xpos,
           red↪ Ypos:(Yneg-Ypos)/24:Yneg);

% Calculate Polar Coordinates Corresponding to Sag Table small Points
        [phi_snsmall,rho_snsmall]=cart2pol(x_sagsmall,y_sagsmall);



% Analytical polynomial Defintions
```

```
        define_power

% Analytical Prescription USing polynomials
        define_prescription

% Define the base asphere for Comparison
        zas=(Cu*rho^2)/(1+sqrt(1-(1+k)*Cu^2*rho^2));

% Define numerical function for the prescription
        poly=matlabFunction(poly);

% Define numerical function for the base asphere
        zasn=matlabFunction(zas);

% Build the numerical domain for the calculation of the surface (polar
   red↪ )
        [X,Y]=meshgrid(-R_CAx:R_CAx/3000:R_CAx,R_CAy1:-((R_CAy1+R_CAy2)
           red↪ /2)/3000:-R_CAy2);
        %[phi_n,rho_n]=meshgrid(0:2*pi/1000:pi*2,-R_CA:R_CA/1000:R_CA);
        [phi_n,rho_n]=cart2pol(X,Y);



% Calculate the surface (polar&cartesian)
        z_presc=poly(X,Y,rho_n);
        z_presc=real(z_presc);
        z_presc_sag=poly(x_sag,y_sag,rho_sn);
        z_presc_sag=real(z_presc_sag);
```

```
       z_prescsmall=poly(x_sagsmall,y_sagsmall,rho_snsmall);
       z_prescsmall=real(z_prescsmall);
% Build the numerical base-sphere surface (polar)
       z_asphere=zasn(rho_n);

% Find the difference between the prescription and the base asphere (
   red↪ polar)
       dzz_sphere=z_presc-z_asphere;
       dzz_sphere=real(dzz_sphere);
% Error from the sag table (Cartesian)
       z_error=z_presc_sag-z_sag;

% Error from the sag table (Cartesian)
       z_errorsmall=z_prescsmall-z_sagsmall;
%write to file
       % xlswrite('nanocam_CPS1_6k_small.xlsx',z_presc);

% Plot the prescription generated surface
    figure(2)
    subplot(2,3,1)
    colormap jet
    contourf(X,Y,z_presc,25)
    title('CPS1 Optical Prescription (mm) ')
    xlabel('x (mm)')
    ylabel('y (mm)')
    set(gca,'FontSize',9)
    axis('square')
```

```
    colorbar;
    C=colorbar;
    C.Label.String = 'z (mm)';

% Plot the deviation of the prescription from asphere
    subplot(2,3,4)
    colormap jet
    contourf(X,Y,dzz_sphere,25)
    title('CPS1 Departure from Base Asphere (mm) ')
    xlabel('x (mm)')
    ylabel('y (mm)')
    set(gca,'FontSize',9)
    axis('square')
    colorbar;
    C=colorbar;
    C.Label.String = 'z (mm)'

% Plot the sag table (loaded)
    subplot(2,3,2)
    colormap jet
    contourf(x_sag,y_sag,z_sag,25)
    title('CPS1 Sag Table (mm) ')
    xlabel('x (mm)')
    ylabel('y (mm)')
    set(gca,'FontSize',9)
    axis('square')
    colorbar;
```

```
    C=colorbar;
    C.Label.String = 'z (mm)'

% Plot the error from the sag table
    subplot(2,3,5)
    colormap jet
    contourf(x_sag,y_sag,z_error*1e06,20)
    title('CPS1 Prescription Error (nm)')
    xlabel('x (mm)')
    ylabel('y (mm)')
    set(gca,'FontSize',9)
    axis('square')
    colorbar;
    C=colorbar;
    C.Label.String = 'error (nm)';

% Plot the sag table (loaded)
    subplot(2,3,3)
    colormap jet
    contourf(x_sagsmall,y_sagsmall,z_sagsmall,25)
    title('CPS1 Sag Table Small (mm) ')
    xlabel('x (mm)')
    ylabel('y (mm)')
    set(gca,'FontSize',9)
    axis('square')
    colorbar;
    C=colorbar;
```

```
    C.Label.String = 'z (mm)'


% Plot the error from the sag tPable
    subplot(2,3,6)
    colormap jet
    contourf(x_sagsmall,y_sagsmall,z_errorsmall*1e06,20)
    title('CPS1 Prescription Error Small (nm)')
    xlabel('x (mm)')
    ylabel('y (mm)')
    set(gca,'FontSize',9)
    axis('square')
    colorbar;
    C=colorbar;
    C.Label.String = 'error (nm)';
```